

ALMA MATER STUDIORUM - UNIVERSITÀ DI  
BOLOGNACAMPUS DI CESENA  
DIPARTIMENTO DI  
INGEGNERIA DELL'ENERGIA ELETTRICA E  
DELL'INFORMAZIONE  
"GUGLIELMO MARCONI"

CORSO DI LAUREA IN INGEGNERIA BIOMEDICA

TITOLO DELL'ELABORATO

ANALYSIS OF THE STATE OF THE ART  
OF THE BIOFABRICATION STRATEGIES  
FOR THE REGENERATION OF THE  
MYOTENDINOUS JUNCTION

Elaborato in

PROPRIETÀ DEI BIOMATERIALI

Relatore:

*Dott. Ing. Alberto Sensini*

Correlatore:

*Chiar.mo Prof. Luca Cristofolini*  
*Chiar.mo Prof. Andrea Zucchelli*

Presentata da:

*Alessia Gualandi*

Anno Accademico 2021-2022

# INDEX

ABSTRACT (Italian).....	3
ABSTRACT (English).....	4
1 INTRODUCTION .....	5
1.1 SKELETAL MUSCLE TISSUE.....	5
1.1.1 HIERARCHICAL STRUCTURE.....	5
1.1.2 MECHANICAL PROPERTIES.....	8
1.2 TENDON TISSUE.....	10
1.2.1 STRUCTURE .....	10
1.2.2 MECHANICAL PROPERTIES.....	11
1.3 MYOTENDINOUS JUNCTION .....	14
1.3.1 STRUCTURE .....	14
1.3.2 MECHANICAL PROPERTIES.....	17
1.4 INJURIES AND SURGICAL TREATMENTS .....	18
1.4.1 MYOTENDINOUS JUNCTION INJURIES .....	18
1.4.2 SURGICAL TREATMENTS .....	20
1.5 SCAFFOLDS AND TISSUE ENGINEERING.....	22
1.5.1 REQUIREMENTS FOR A SCAFFOLD .....	23
1.6 ELECTROSPINNING .....	26
1.7 3D PRINTING .....	32
1.9 MATERIALS.....	35
2 AIM OF THE THESIS .....	37
3 METHODS OF THE RESEARCH STRATEGY .....	38
4 RESULTS OF THE LITERATURE SEARCH.....	39
4.1 ELECTROSPINNING .....	39
4.2 3D-PRINTING.....	58
4.3 CONSTRUCTS ENGINEERED IN VITRO .....	68
5 DISCUSSIONS.....	71
7 REFERENCES .....	74
RINGRAZIAMENTI.....	80

## **ABSTRACT (Italian)**

La giunzione miotendinea (MTJ) è una struttura anatomica specializzata che collega il muscolo al tendine. La sua funzione è quella di permettere la trasmissione della forza generata dal muscolo al tendine, permettendo il movimento. Essendo una struttura di interfaccia che funge da raccordo tra due tipi di tessuti molto differenti, tende a risentire di una forte concentrazione di tensione, questo la rende fortemente suscettibile a rottura.

Le tecniche ad oggi utilizzare per riparare lesioni alla MTJ risultano inadatte ad una completa ed ottimale ripresa meccanica. Al fine di trovare una soluzione a questo problema, l'ingegneria tissutale sta lavorando alla fabbricazione di strutture tridimensionali che siano in grado di imitare al meglio la struttura nativa della MTJ.

Le tecniche utilizzate per la produzione di tali strutture sono, principalmente, stampa 3D ed elettrofilatura. Il vantaggio di queste tecniche è la loro elevata risoluzione, che permette di controllare finemente l'architettura di tali strutture artificiali.

Nella seguente tesi verrà presentato lo stato dell'arte sulle tecniche utilizzate per la fabbricazione di scaffolds per la rigenerazione della MTJ, soffermandosi in particolare sui metodi di fabbricazione e sulle prestazioni morfologiche, meccaniche e cellulari effettuando un confronto tra i diversi studi che se ne sono occupati, individuandone punti di forza, debolezze e possibili studi futuri che potranno essere effettuati su tali scaffolds. In questo modo, sarà possibile rendersi conto di quale di queste tecniche risulti essere più promettente per il futuro.

## **ABSTRACT (English)**

The myotendinous junction (MTJ) is a specialized anatomical structure that connects muscle to tendon. Its function is to allow the transmission of force generated by the muscle to the tendon, enabling movement. Being an interface structure that allows the junction between two very different types of tissues, it tends to suffer from a high stress concentration, which makes it highly prone to injuries.

The techniques currently used to repair injuries to the MTJ are unsuitable to improve its mechanical recovery. To find a solution to this problem, tissue engineering is working on the biofabrication of three-dimensional structures that can better mimic the native structure of the MTJ.

The techniques used to produce such structures are, primarily, 3D printing and electrospinning. The advantage of these techniques is their high resolution, which allows a fine control of the architecture of such artificial structures.

The aim of the thesis is to investigate the techniques used for the biofabrication of scaffolds for MTJ regeneration comparing the different studies that have dealt with it, analyzing their positive and negative aspects. In this way, it will be possible to realize which of these techniques is more promising for the future.

# **1 INTRODUCTION**

## **1.1 SKELETAL MUSCLE TISSUE**

### **1.1.1 HIERARCHICAL STRUCTURE**

In general, there are three different types of muscle tissue in the human body: smooth muscle, cardiac muscle, and skeletal muscle. Cardiac and skeletal muscles are made up of striated muscle fibers, while the smooth muscle is made up of smooth muscle fibers. The difference between skeletal and cardiac muscle is that cardiac muscle fibers are controlled by the involuntary nervous system (as are those of smooth muscle), while those of skeletal muscles are controlled by the voluntary nervous system [1].

Smooth muscle tissue is found in the blood vessels, digestive system, bronchioles, uterus, and bladder; while skeletal muscle tissue is what allows for the voluntary movements of the body [2]. With MTJ, the muscle tissue involved is skeletal muscle tissue.

As well as many other tissues, muscle tissue is hierarchically organized (Fig.1). The muscular fiber (10-100 $\mu$ m) is its constitutive contractile unit. It is composed of a polynuclear cell called a myocyte. Each myofiber is surrounded by a membrane called endomysium. Several myofibers are grouped generating the muscle fascicle (0.5-30mm); each fascicle is surrounded by a membrane of connective tissue, called perimysium, which provides pathways for blood vessels and nerves. Several fascicles form the actual MT, surrounded by a dense connective tissue, called epimysium, which facilitates muscles sliding along each other, and supports the structural and functional continuity of the muscle-tendon joint. Just behind the epimysium lies the sarcolemma, a thin layer of elastic covering [3].

The skeletal muscle tissue is predominantly composed of water, protein (such as collagen, myosin, actin, and titin [4]), minerals, fat, and carbohydrates.

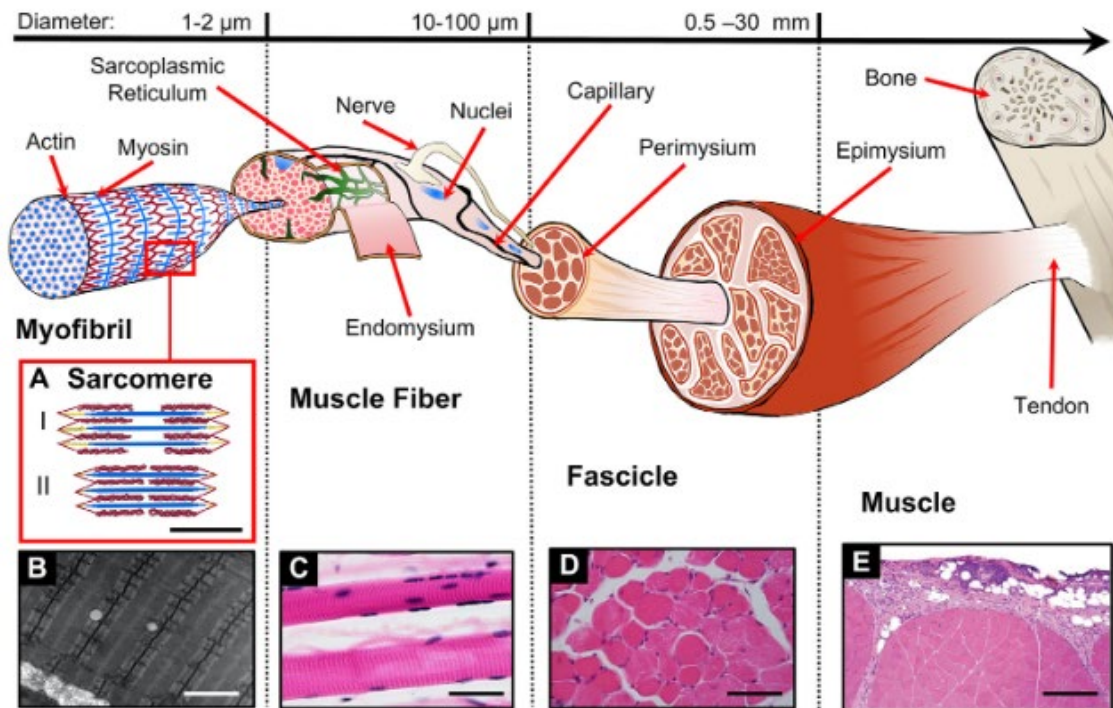


Fig.1 Hierarchical structure of skeletal muscle. A) Sarcomere morphology and sliding mechanism (Scalebar 0.5 nm): Actin (red), Myosin (blue), and Titin (yellow) filaments are shown in the relaxed state (I) and during the contraction (II). The jagged sides represent the Z-lines. The central space without actin filaments is the H zone. B) Transmission Electron Microscopy (TEM) image of myofibrils (scalebar = 1 nm). C) Phase Contrast Microscope (PCM) image of skeletal muscle fibers. Dark violet elliptical elements are the myocytes nuclei (scalebar = 50 μm). D) Histological image of a fascicle cross-section. Larger white bands are the perimysium membranes. Circular structures are the muscle fibers, while the darker violet dots are the myocytes nuclei (scalebar = 100 μm). E) Histological image of a portion of muscle cross-section. In the upper part, the epimysium membrane is visible (scalebar = 0.5 mm) [5].

At the ultrastructural level, the major components of myofibers are the myofibrils (1-2μm). Myofibrils are divided into contractile units, called sarcomeres, that are delimited by Z lines. It is the smallest functional unit capable of contracting. Sarcomeres are arranged in series along the length of the fiber, hundreds of sarcomeres in series give the typical striated appearance of the muscle fiber. Each sarcomere consists of thick filaments, thin filaments, and accessory proteins (such as titin and nebulin) [6].

The thick filaments are made up of myosin molecules, each of which consists of two light chains in turn associated with two heavy chains. The heavy chains have a globular head and an alpha-helical tail. Each myosin head has two specific sites, one for actin, which connects thick and thin filaments, and one for ATP, whose hydrolysis provides the energy needed for contraction. Within the sarcomere, the myosin molecules are arranged so that the tails are in the center, while the heads face left and right in a mirror-like fashion. The myosin filaments are anchored in the center of the sarcomere at the M line.

The thin filaments are made up of several proteins (actin, troponin, and tropomyosin). Actin serves as the skeleton of the filament; it is present as a double-helix polymer and has a binding site for myosin. Tropomyosin is arranged along the actin filament covering all the binding sites for myosin. Troponin has three subunits, the C subunit has four calcium-binding sites, the T subunit binds tropomyosin and the I subunit has inhibitory functions.

Accessory proteins determine the length of the thin filaments and the passive force of the muscle.

The force developed by the muscle depends on the degree of filament overlap, which varies with sarcomere elongation.

The central zone of the sarcomere, where the myosin is situated, is called A-band; the area which contains only actin is called the I-band, while the H-band is the area at the center of the A-band where there is only myosin. The movement of the myosin heads slides actin filaments towards the center of the sarcomere, thereby shortening the sarcomere and the muscle fiber, to generate force. Skeletal muscles' activation is performed under voluntary or reflex control of the central nervous system and peripheral nerves, in contrast to smooth and cardiac muscles, which are subject to involuntary control by the vegetative nervous system [3]. Depending on their speed of contraction, biochemistry, and ultrastructure, they can be delineated into two basic types of skeletal muscle: slow-twitch fibers (type I) and fast-twitch fibers (type II). Muscles are composed of a mixture of fiber types.

### 1.1.2 MECHANICAL PROPERTIES

Skeletal muscle is the most dynamic and abundant tissue in the human body, representing approximately 40% [7] of its mass and 50-75% of its protein content. From a mechanical point of view, the main function of skeletal muscle is to convert chemical energy into mechanical energy, applied to the bone via the tendinous tissue. Other functions of the skeletal muscle are to maintain posture and supporting soft tissue.

There are many other functions, such as locomotion, breathing, protecting internal organs, and coordinating global energy expenditure [8].

It has a Young-Modulus around  $11.1 \pm 4.10$  kPa depending on the type of muscle and age [9].

The muscle has a strain capacity that changes depending on whether the required motor task is active or passive (a passive task is greater than active). Applying an increasing load, the stress-strain curve has a first almost elastic-linear region. Once the yield stress is reached, the muscle assumes a non-linear stress-strain pattern until it reaches rupture.

In contrast to the tendon, muscle is decidedly less rigid (it has a low Young-Modulus) and has a decidedly lower tensile stress at rupture, but due to its high percentage of elastin, it has good deformation at rupture (Fig.2).

Another determining factor influencing muscle mechanical properties is the speed of load application. Increasing the speed of load application increases the Young Modulus.

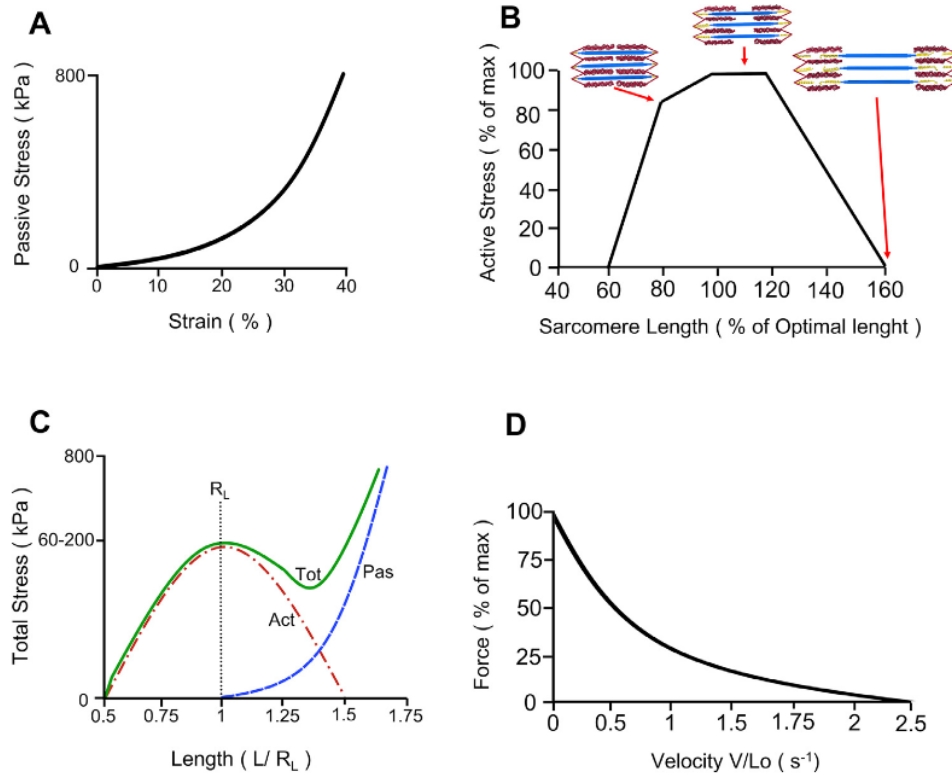


Fig.2 Passive and active mechanical behaviors of skeletal muscles. A) Typical passive stress-strain curve. B) Typical sarcomere active stress (expressed as a percentage of the maximum) compared to the sarcomere length (expressed as a percentage of its optimal length). The active stress is maximum in correspondence to the sarcomere optimal length  $L_0$ . The pictures show the different levels of sarcomere overlap. C) Total stress-length behavior during a contraction. Length is normalized by the resting length ( $R_L$ ) of the muscle. The total curve (Tot) is the composition of the active curve (Act) and the passive one (Pas). The active curve finds its maximum in correspondence to the optimal length of the sarcomere ( $R_L$ ). D) Typical force (expressed as a percentage of the maximum) compared to the speed of contraction (normalized by the optimal length of the sarcomere) [5].

**Table 1:** Typical ranges of animal skeletal muscle passive mechanical properties [5].

	<b>Young Modulus [kPa]</b>	<b>Failure Strain [%]</b>	<b>Failure Stress [kPa]</b>	<b>References</b>
<b>Myofibril</b>	25-40	30-60	---	[10-14]
<b>Fiber</b>	20-100	30-60	430-1973	[14-20]
<b>Whole Muscle</b>	30-8000	30-60	70-800	[12,19,21-24]

## 1.2 TENDON TISSUE

### 1.2.1 STRUCTURE

Morphologically speaking, tendons are a hierarchical structure of dense, parallel, connective tissue bands that span a joint connecting bone to muscle.

The basic unit of tendons is the tropocollagen molecule, which is a long, thin protein produced inside a cell and secreted into ECM as procollagen. Tropocollagen molecules aggregation produces the collagen fibril, which is the smallest structural unit of the tendon tissue. The diameter of the fibrils ranges from 10-500nm, depending on species, age, and anatomical location [25].

Tendons are assembled from cross-linked tropocollagen molecules aggregated progressively into fibrils, primary fiber bundle (subfascicle), secondary fiber bundle (fascicle), and tertiary fiber bundle. Several tertiary fiber bundles form the tendon, which is surrounded by the epitenon. The structures from fibers to tertiary fiber bundles are surrounded by a thin collagen membrane, called endotenon, containing blood vessels, lymphatics, and nerves [25,26] (Fig.3).

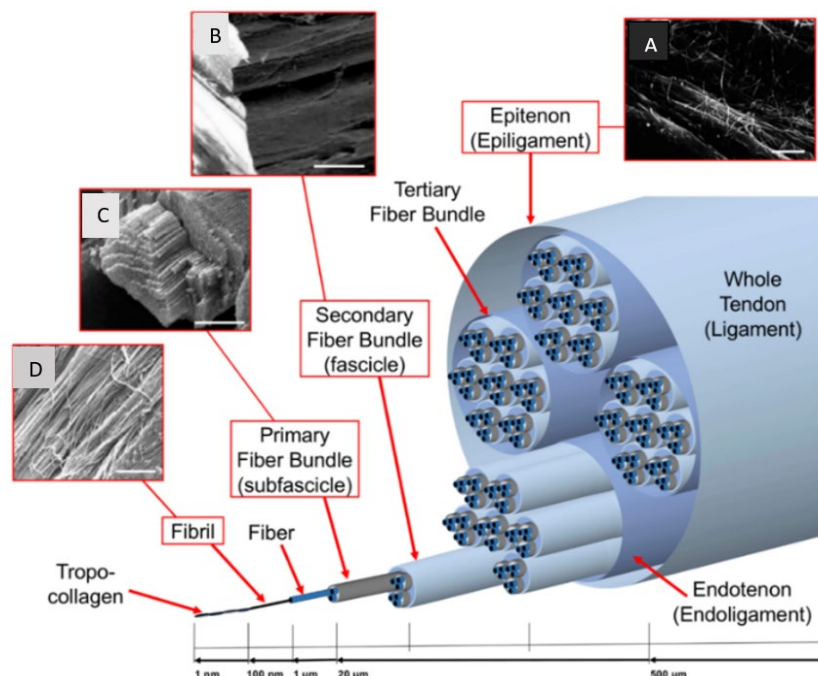


Fig.3 Hierarchical arrangement of the collagen of tendons: (A) Scanning electron microscopy (SEM) of epitenon collagen fibrils (scale bar = 2 micrometers); (B) SEM image of a collagen fascicle (scale bar = 100 micrometers); (C) SEM image of a collagen bundle (scale bar = 45 micrometers); and (D) SEM image of collagen fibrils (scale bar = 1.8 micrometers). (B-D) SEM images. [25].

This hierarchical structure provides the tendon with high tensile force and resilience while preventing damage and separation of the fibers under mechanical stress.

Tendons consist of few cells and abundant ECM. The cellular component, primarily consisting of tenocytes, comprises 20% of the total tissue volume, whereas the ECM accounts for the remaining 80% [27]. Approximately 70% of the ECM is water, which helps modulate cellular function and viscoelastic behavior. The remaining 30% of the ECM is composed of solids, such as collagen and ground substance. The ground substance (a non-fibrous component of the matrix) primarily comprises hyaluronan, glycoproteins, and proteoglycans and modulates tissue metabolism, provides shock absorption, decreases internal friction, and binds water. The fibrous component, which comprises 75-80% of the dry weight of tendons, provides strength and a supportive structure and consists primarily of type I collagen. Smaller amounts of type III, VI, V, XI, and XIV collagens are also present [26].

### **1.2.2 MECHANICAL PROPERTIES**

Tendons with muscles move or stabilize joints. Tendons must therefore exhibit nonlinear mechanical behavior that is relatively flexible under low loads and rapidly stiffens under higher loads. This passive elastic behavior is accompanied by time-dependent behavior.

The mechanical behavior of a tendon provides a clear understanding of its normal function and mechanisms of injury. The strength of a tendon under a uniformly distributed load is largely determined by the cross-sectional size of the tissue and the magnitude of the load. Tendons show increased strength and stiffness with an increased loading rate. The structural properties of tendons are typically collected by tensile testing at a constant increase in strain and displayed on a force-elongation curve. From the force-elongation data, a nominal stress-strain relationship is determined to provide the average mechanical properties of the fabric.

The nominal stress is the force divided by the original cross-sectional area of the tendon and the nominal strain is the stretched length of the ligament minus its original length and divided by its original length. The calculated stress-strain curve identifies the commonly reported Young Modulus, tensile strength, and strain (Fig.4) [26].

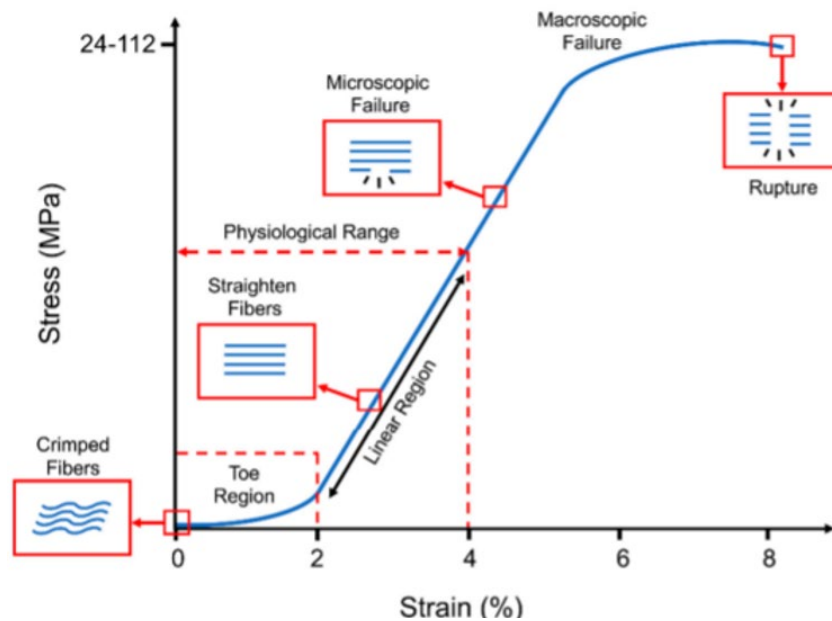


Fig.4 Typical stress-strain curve and schematization of the behavior of the collagen fibers for tendons. Typical ranges of stress and strain are indicated on the x and y axes [25].

The resulting force-elongation (or stress-strain) curve separates the tissue behavior into three regions, called: the toe, linear, and rupture regions. Within the toe region, the collagen fibers of the unstressed tendon are compounded in a wavelike pattern. The mechanism that causes the collagen fibers to curl is not well understood, but the curled fibers provide minimal resistance to movement over an initial range of stresses. The crimp region is very flexible. As the tendon is loaded, the fibers straighten, and the wave pattern is lost. As loading continues, the stiffness of the tendon increases and a greater force is required to produce an equivalent increase in strain. Once the strain increases to 1.5-4%, nearly linear stiffness is observed. When strain is further increased beyond the linear range (8-10 % strain), fiber ruptures, and eventually complete and irreversible failure occurs [28].

The irreversible damage begins about halfway through the linear region, after which the original length can no longer be recovered by removing the load.

The viscoelastic behavior of tendons aids and protects joint function. Viscoelasticity adds time dependence to the elastic phenomena described. It manifests itself by allowing easier joint movement after elongation, increasing the strength of the tendon to resist impact forces, and absorbing some of the energy in dynamic loads [29]. These behaviors can be quantified by creep and relaxation testing. If a tendon is held at a constant strain, it shows relaxation, which means that the load decreases over time (Fig.5A). The tendon also shows creep where the strain increases over time under a constant tensile force (Fig.5B). When a tendon is subjected to a higher rate of loading, the linear portion of the stress-strain curve becomes steeper, indicating greater stiffness and loading of the tissue before reaching the breaking strain.

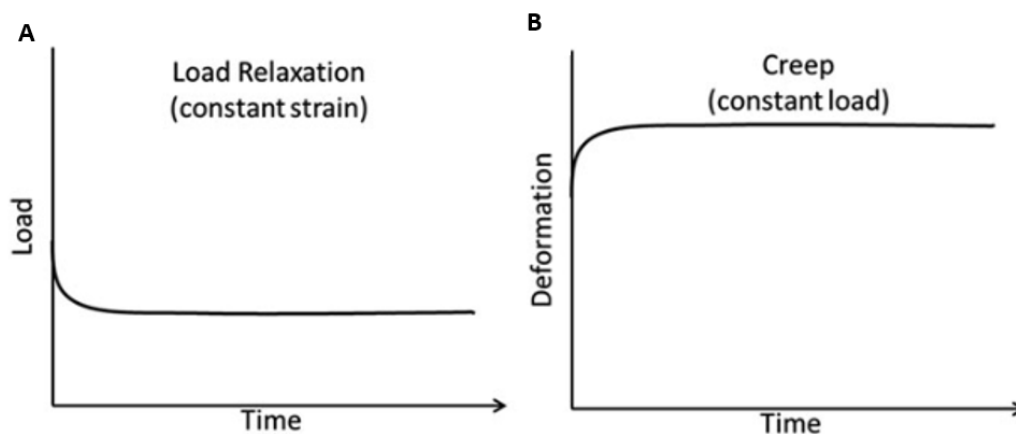


Fig.5 Viscoelastic properties of ligaments are demonstrated by load relaxation (a) and creep (b). Load relaxation is demonstrated by loading the ligament (below the linear region) and maintaining constant strain over an extended period. Load decreases rapidly and then continues at a low rate (a). Creep takes place when the ligament is loaded (below the linear region) at a constant level over time. As a result, deformation increases quickly at first and then continues at a low rate[26].

## **1.3 MYOTENDINOUS JUNCTION**

### **1.3.1 STRUCTURE**

The muscle can transmit its force to the bones using tendons, the complex structure of connective tissue, which connects the muscle to the bone tissue. These tissues have a very different composition from each other, causing a high concentration of stress where there is a variation of tissue types. To avoid too high concentrations, the human body has implemented a series of measures, both in the tendon-bone connection and in the tendon-muscle connection.

The myotendinous junction (MTJ) is a specialized anatomical region in the musculotendinous system that connects skeletal muscle to the tendon, providing a smooth transition between tendon and muscle tissue [4].

Tissues in the musculoskeletal system are structurally optimized to efficiently transfer the force generated in the muscle through the tendon to the bone to produce movement. This load must be seamlessly propagated through tissues with disparate biological and mechanical properties via distinct tissue interfaces. Thus, developing methods by which to fabricate composite structures is an important step in the engineering of increasingly complex tissue constructs [30,31]. One opportunity for engineering complex musculoskeletal tissues is for the design and fabrication of the MTJ. While many attempts have been made to engineer muscle [32,33] and tendon separately, few attempts have focused on engineering the composite structure. The native MTJ is made up of three distinct regions: muscle which is elastic and predominantly made up of multinucleated myofibers; tendon which is stiff and predominantly made up of collagen and sparse fibroblasts; and a muscle-tendon junction (MTJ) which is a complex cell-matrix interaction between the cell-rich muscle side and the extracellular matrix (ECM)-rich tendon side. Mechanically, muscle has elastic properties to allow for contraction and relaxation, while the tendon is a stiff material that allows for the efficient transmission of force onto its bony insertion.

Thus, a tissue-engineered MTJ construct would similarly have three distinct regions: an elastic region on the muscle side populated by muscle cells, a stiff region on the tendon side populated by tendon cells, and a junction region that connects the two sides into an integrated unit.

The stress generated by muscle fibers is transmitted from their intracellular contractile proteins to the extracellular connective proteins in the tendon.

Skeletal muscle and tendon are complex, neighboring tissues with their own specialized structural, mechanical, and functional properties. Since what gives the muscle contractility is its cellular component, while what gives the tendon its strength is the extracellular component, a specific interface is required to connect the two different tissues [34]. To effectively transmit the force generated from the intracellular contraction of the muscle proteins to the extracellular collagen fibers of the tendon, the MTJ requires contiguous transmembrane connections. Furthermore, the difference between the mechanical properties of tendon and muscle at the MTJ interface makes it more subject to damage [9]. The muscle is the most flexible of these tissues, but also the thinnest at its insertion with the tendon. It submits the MTJ to the greatest stress and exposes this area to rupture.

At the macroscopic scale, the muscle-tendon interface is not a well-defined separation. Muscle and tendon tissues meet in a zone where they overlap, resulting in a gradient in tissue composition. At the microscopic level, the major structural features of the MTJ are the interdigitations of the sarcolemma with the tendon ECM. Consequently, the interdigitations known as “finger-like” greatly increase the contact area between the two types of tissues by 10 to 50 times (Fig.6). This feature enables MTJ to reduce the stress-concentration generated by muscle contraction [35] and consequently the risk of rupture [3].

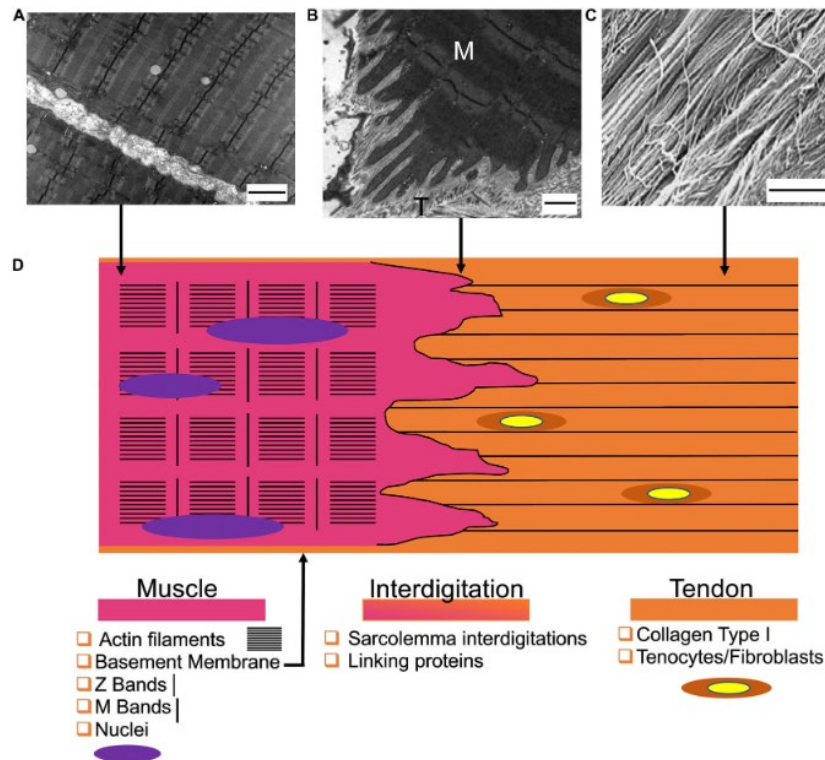


Fig.6 Structure of the myotendinous junction. (A)Transmission electron microscopy image of myofibrils (scale bar = 2μm). (B)Transmission electron microscopy of the MTJ of the rat sternomastoid muscle (M = muscle side; T = Tendon side) (scale bar = 0.5μm). (C) View of the tendon fibers observed with SEM (scale bar = 1.8μm). (D) Graphical representation of the MTJ and its components [4].

Finger-like processes are interdigitations of the sarcolemma, where actin filaments that extend from the last Z line are connected to the subsarcolemmal proteins and indirectly interact with extracellular components. The size of finger-like processes differs among animal species and spatial changes may occur with exercise and aging. Interdigitations shorten with aging and the contact area between sarcolemma and extracellular components decreases resulting in muscular atrophy. Their size differs also between the two muscle fiber types. Interdigitations are wider in slow muscle fibers than in fast muscle fibers. Two separate transmembrane-linkage systems have been described in the MTJ. Both constitute a structural link between cytoplasmic actin and tendinous ECM proteins via laminin 211. The first linkage system contains the dystrophin-associated glycoprotein complex (DGC) and the second the  $\alpha7\beta1$  integrin. Integrins are the major membrane receptors of ECM proteins [36].

Adhesive complexes are essential for MTJ function since they are responsible for transmitting mechanical forces, maintaining, and securing skeletal muscle fibers to tendon fibrils.

### 1.3.2 MECHANICAL PROPERTIES

The mechanical properties of MTJ were evaluated by isolating it and subjecting it to mechanical uniaxial stress tests using the testing machine, after recording its initial width and thickness. The mechanical test involved stretching it to failure (in stress) at a rate of 10mm/min. Thanks to this test, it was possible to obtain the mechanical properties such as Young Modulus, ultimate tensile strength, and ultimate strain of the MTJ [table 2] [37].

The mechanical properties of the MTJ are similar to those of muscle on the muscle side and similar to those of the tendon on the tendon side. The purpose of the MTJ is to make a smooth transition between these two tissues. Therefore, its mechanical properties are intermediate between those of tendon and muscle (Table 2).

**Table 2:** Mechanical properties of the native MTJ [37].

	<b>Distal Aponeurosis</b>	<b>Proximal Aponeurosis</b>
<b>Failure stress (MPa)</b>	32.07 ± 8.26	46.98 ± 10.04
<b>Young Modulus (MPa)</b>	79.13 ± 9.38	126.05 ± 40.42
<b>Failure strain</b>	0.55 ± 0.12	0.40 ± 0.09

**Table 3:** Ranges of mechanical properties of the different musculoskeletal tissues [4].

	<b>Failure strain [%]</b>	<b>Failure stress [MPa]</b>	<b>Stiffness [MPa]</b>	<b>References</b>
Tendon (human)	9-55.5	7.3-116	99.6-926	[38,39]
Muscle (human)	30-60	0.07-0.8	0.03-8	[13,14,19,40-46]
Diaphragm (pig) MTJ	122.4 ± 19.2	0.15 ± 0.02	0.28 ± 0.15	[47]
Achilles tendon-triceps surae (pig) distal MTJ	45-75	20-40	90	[37]
Achilles tendon-triceps surae (pig) proximal MTJ	35-55	40-60	70-150	[37]

## **1.4 INJURIES AND SURGICAL TREATMENTS**

### **1.4.1 MYOTENDINOUS JUNCTION INJURIES**

Since the MTJ is located at an interface between two different tissue types, it is subjected to a high concentration of stresses that make it susceptible to injury.

All tendons have the potential to be affected by direct damage caused by accidental lacerations, or through participation in sports. They can be susceptible to diseases such as osteoarthritis. Tendon diseases were previously assumed to be caused by inflammation of the tissue and were termed “tendonitis”. However, it was later discovered that the avascularity of tendons does not predispose the tissue to inflammatory processes and thus tendonitis is a misconception [27].

Clinically, tendon disorders are commonly referred to as a ‘tendinopathy’ as this does not assume the pathological processes within the tendon.

The injuries at the MTJ are classified in three degrees. First-degree injury relates to limited injury or edema that heals without permanent consequences. In second-degree injury, there is a partially broken MTJ, which causes severe pain to the patient and can result in repeated recurrent injury. A conservative approach is used to treat this type of injury, which restores muscle strength and range of motion. The third degree is related to the total rupture of the MTJ. The surgical approach to managing the third degree (total rupture) depends on several factors such as the patient’s age, the rupture site, and the actual range of motion [4].

MTJ injuries often involve older people or young athletes. It is very important to consider MTJ injuries, as 73% of injuries considered muscular, actually involve the MTJ. In addition, 66% of MTJ injuries occur due to sports, among other causes of injuries we have accidents at work, car accidents, and moving heavy objects [48].

Of all injuries affecting the musculoskeletal system, 28% involve the MTJ. The average age of patients in whom MTJ injuries have occurred is approximately 38 years (Fig.7) [48].

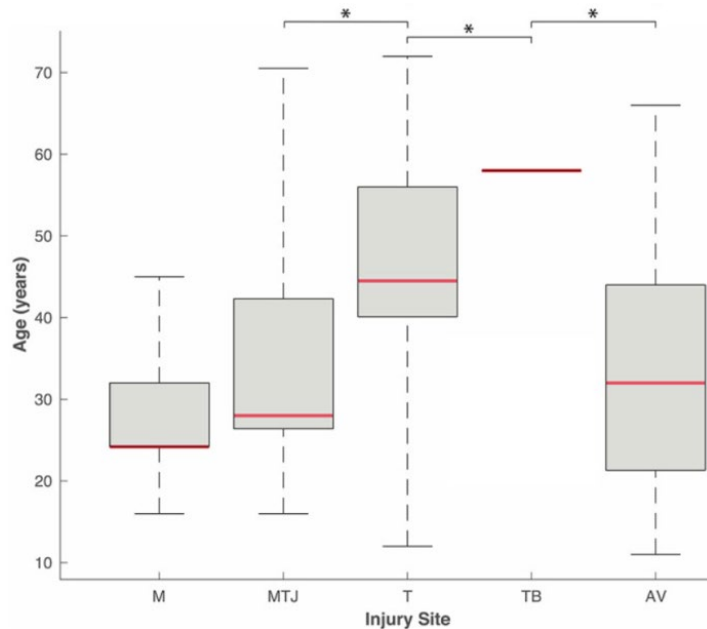


Fig.7 Box-and-whisker plot of patient age by injury site (n=2.106). \*P<0.001. One-way analysis of variance. AV=tendon avulsion; M=muscle belly; MTJ=myotendinous junction; T=tendon; TB=tendon-bone junction [48].

MTJ injuries occur predominantly in the following areas: biceps femoris; supraspinatus and Achilles tendon (Fig.8). The biceps femoris was the most injured musculotendinous unit, representing 25.1% of the injuries. Of those, 14.4% were in the MTJ, and 9.7% were in the muscle belly [48].

There were 3 muscle groups more predominantly involved: the hamstring, the quadriceps, and the rotator cuff. From the hamstring group, the biceps femoris was the most frequently injured (25.1%); from the quadriceps group, the rectus femoris was the most injured unit (3.1%); and from the rotator cuff, the supraspinatus was the most prone to injury (11.7%) [48].

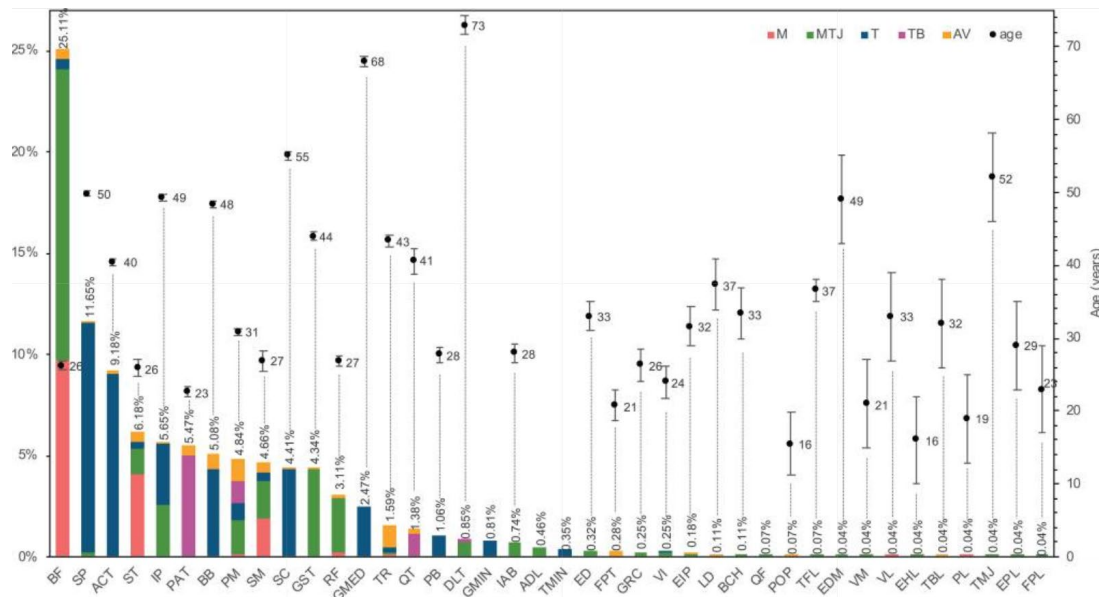


Fig.8 Injury distribution by muscle/tendon and injury site (n = 2,832) and mean  $\pm$  SEM age by muscle/tendon (n = 2,106). Patient age was not reported for ADL, TMIN, and QF injuries. ACT, Achilles tendon; ADL, adductor longus; AV, tendon avulsion; BB, biceps brachii; BCH, brachialis; BF, biceps femoris; DLT, deltoid; ED, extensor digitorum; EDM, extensor digiti minimi; EHL, extensor hallucis longus; EIP, extensor indicis proprius; EPL, extensor pollicis longus; FPL, flexor pollicis longus; FPT, flexor profundus tendon; GMED, gluteus medius; GMIN, gluteus minimus; GRC, gracilis; GST, gastrocnemius; IAB, internal abdominal; IP, infraspinatus; LD, latissimus dorsi; M, muscle belly; MTJ, musculotendinous junction; PAT, patellar tendon; PB, peroneus brevis; PL, peroneus longus; PM, pectoralis major; POP, popliteus; QF, quadratus femoris; QT, quadriceps tendon; RF, rectus femoris; SC, subscapularis; SM, semimembranosus; SP, supraspinatus; ST, semitendinosus; T, tendon; TB, tendon-bone junction; TBL, tibialis posterior; TFL, tensor fasciae latae; TMIN, teres minor; TMJ, teres major; TR, triceps brachii; VI, vastus intermedius; VL, vastus lateralis; VM, vastus medialis [48].

## 1.4.2 SURGICAL TREATMENTS

There are different surgical solutions to third-degree MTJ injuries, like sutures and grafts.

In traumatic injuries, where the muscle-tendon interface is completely separated, the simple suture has been shown to not provide adequate functional recovery because the sutured region doesn't have the same mechanical properties as the native region [4].

Grafts can be divided into three categories, which are distinguished by the type of donor: allograft, autograft, and xenograft.

Autograft comes from the patient himself. The advantage of this graft is that it doesn't incur rejection because the cells that constitute it are not considered extraneous. The disadvantage is that it causes a collateral injury.

The allograft comes from corpses, while xenograft comes from animals with similar tendinous structures. The advantage is that they don't cause collateral injuries, but they need to be decellularized to avoid rejection. Decellularization worsens their mechanical properties and requires a longer recovery time because of cell repopulation.

The use of autografts is currently the only gold standard method for managing large tendon deficits [49,50]. However, reconstruction of such large defects requires massive tissue harvesting from the donor site, and therefore the donor site morbidity and pain is a considerable challenge to autografts [50–52]. In addition, there may not be enough autografts in the patient's body at the time of reconstruction. Another limitation of this treatment strategy is that it is often necessary to make a second surgery on the patient which increases the surgical time and cost [53].

In contrast to autografts are allografts and xenografts [54,55]. Allografts have lower immunogenicity than xenografts, but both have this chance to be acutely or chronically rejected by the host [50]. In addition, it has been stated that using allografts or xenografts increases the chance of disease transmission of several hazardous and dangerous viruses and prions such as human immune deficiency virus, hepatitis type B, and more importantly types C and bovine spongiform encephalitis [49–51,56]. Disease transmission in xenografts is a more serious concern than in allografts because there are well known human diseases that could be detected in the allografts using the standard screening technologies but in xenografts, there are several unknown zoonotic diseases that are more hazardous to the human body than those of the well-known humane diseases [50,51,56]. In addition to these disadvantages, there are also several ethical concerns regarding the use of allografts and xenografts in the human body [54,55].

Comparing auto- to allografts and xenografts options, autografts have better incorporative properties than the other grafts because basically the autografts are viable tissues, and their cells can collaborate at different stages of healing [51,57,58]. In addition, the resorption rate of autografts is lower than other grafts; therefore, the healing in autografts would be faster [51,59]. In contrast to autografts, the most important positive and beneficial issue regarding allografts and xenografts is their availability [53,55]. To reduce the immunogenicity of allografts and xenografts, various procedures such as sterilization and decellularization have been applied, resulting in a deterioration of their mechanical properties. Therefore, it is a fact that the allografts and xenografts have significantly lower incorporative properties than the healing tissue, and this is another major limitation that results in rapid absorption of the graft during tendon healing [59–61].

Due to the several limitations of the surgical solutions, researchers focused on the production of synthetic scaffolds able to mimic the MTJ structure and mechanics. This branch of tissue engineering is named “Interfacial Tissue Engineering” [62].

## **1.5 SCAFFOLDS AND TISSUE ENGINEERING**

Tissue Engineering (TE) is a biomedical engineering discipline that uses cells and materials to restore, replace or improve different types of biological tissues. Scaffolds represent the main resource of TE; they are artificial structures with nanometer morphological characteristics engineered to emulate the ECM in order to support cell cultures and promote their growth until regeneration of damaged tissue is achieved.

TE is a promising approach to repair tendon and muscle when natural healing fails. Biohybrid constructs obtained after cells’ seeding and culture in dedicated scaffolds have been considered relevant tools for mimicking native tissue, leading to better integration *in vivo*. They have been employed to perform advanced *in vitro* studies to model cell differentiation or regeneration processes [3].

Engineering a tissue for MTJ repair is a complex task, in link with the complexity of the native tissue. The MTJ is not a smooth continuous division between muscle and tendon to limit stress-associated failure. The gradient of structural and mechanical properties throughout the entire interface region should be replicated to mimic its functions. In addition, this tissue is always submitted to mechanical passive and active strains, which probably contribute to its specific structure. Therefore, to properly engineer a composite muscle-tendon system, those very specific biological, biomechanical, and structural properties of the muscle fibers, tendon and interface must be accounted for [3].

### **1.5.1 REQUIREMENTS FOR A SCAFFOLD**

Considering the morphology and the mechanical properties previously described the general requirements for a scaffold for the regeneration of these tissues are:

- a. **Biocompatibility:** scaffolds can be made of natural or synthetic materials and must be biocompatible. This feature is of paramount importance as it increases the ability of cells within the scaffolds to grow, infiltrate and proliferate. Biocompatibility is very useful in preventing and minimizing inflammatory phenomena that can compromise the regenerative process [50,60,63].
- b. **Biodegradability:** scaffolds must be able to be degraded by cells and body fluids over time. Their biodegradability must be such that cells can reproduce natural collagen without it being reabsorbed too quickly. It is critical that the products of scaffold degradation do not have inflammatory or toxic effects on surrounding cells and tissues [50,60,63].
- c. **Mechanical properties:** for the injured tissue to be effectively replaced, cells must be able to feel the physiological stiffness of the substrate and be affected by physiological levels of strain. The cells must feel stimulated to reproduce collagen and proliferate [25,50,60][50]. These are the reasons why scaffolds must be designed to provide mechanical properties like those of native tissue.

There is a need for scaffolds to be less rigid and less strong than native tissue to avoid damage to surrounding tissues. In addition, some degree of ductility is required before nominal loading to avoid unexpected and abrupt failure of the structures when overloaded. In this way, it will be possible to realize that the structure is failing before it finally breaks.

- d. Morphology: a scaffold designed for the regeneration of a structure like the MTJ must reproduce as best as possible the original structure of the native MTJ. On the one hand, it should be able to reproduce the highly hierarchical structure of tendons and muscles, on the other hand, it should be able to develop the typical interface interdigitations between the two tissues. Fiber-like scaffolds allow for better cell adhesion and growth and collagen reproduction that follows the direction of fiber alignment, allowing for the typical mechanical properties of this structure precisely because of the morphology [25].
- e. Porosity: the scaffolds must be porous to allow cellular infiltration [60,64]. The porosity follows one another forming a real network inside the scaffold, which allows cells to feed, proliferate and migrate and promotes vascularization and the formation of new tissues. Materials with high porosity allow the release of biological factors such as genes and proteins, providing good substrates for the exchange of nutrients between cells [65–69].

Tissue scaffolds can be classified into three different categories based on their origin: biological, synthetic, or hybrid [60].

Among the main biological scaffolds, we have those coming from cadavers, while the most recent ones are formed by molecules based on elastin, collagen, chitosan, etc. [60]. Synthetic scaffolds, in contrast to biological ones, are obtained by polymerization of synthetic materials [56,60]. The most widely used are those consisting of polypropylene, polycaprolactone, nylon, hydroxyapatite, etc. [50,56].

One of the main goals of tissue engineering related to tendons is to obtain scaffolds that simulate the characteristics of the native tendon in a short time, but it is also important that these structures can be gradually degraded and resorbed (replaced by new tissue). The two different types of scaffolds previously described have different advantages. Synthetic scaffolds have higher mechanical properties than biological ones; therefore, they are more suitable in the short term; while biological scaffolds have lower mechanical properties, but in the long term they are the best choice [50,56].

This is since the mechanical properties of biodegradable scaffolds decrease with time and if new tissue could not be developed to completely replace the graft, the breakage could occur [60].

To overcome the difficulties of biological scaffolds in the short term and those of synthetic scaffolds in the long term, scientists invented hybrid scaffolds, consisting of a combination of synthetic and biological materials. This allowed them to increase their biodegradability, biocompatibility, mechanical properties, and healing incorporative characteristics.

It is possible to increase the mechanical properties of biological scaffolds through fiber cross-linking. To date, there are several fiber cross-linking techniques, including chemical cross-linking, dehydrothermal cross-linking, and ultraviolet cross-linking [56,60].

Ultraviolet cross-linking appears to be the safest and most effective, as it does not involve deleterious effects on the body, unlike the alternatives. Chemical cross-linking can cause harm as the chemical solution used tends to remain bound to the scaffold and this is harmful to the body [56]. Dehydrothermal cross-linking is harmful as it tends to decrease the biodegradability of the scaffold [60].

It is very important to use fiber cross-linking as otherwise the scaffold will be water-soluble and will be absorbed by the host immune response.

Comprehensive detailed studies have shown that it is better to construct the main part of the scaffold with biological-based materials such as collagen and cover it with synthetic-based scaffold such as polydioxanone [56].

In addition to the features just described, scaffolds' architecture is also very important. Tendons are highly aligned tissues with unidirectionally arranged structural units and are densely packed. These tissues are composed of nano and micro collagen fibers, so it is important to be able to reproduce aligned scaffolds and it should have both micro-nano-scaled fibers in its architecture [50,60].

To reproduce this type of architecture, the best solution seems to be the use of a new technique, called electrospinning.

## **1.6 ELECTROSPINNING**

Electrospinning is a technique that allows the production of fibers with diameter in the nanoscale. It is an innovative technique that is finding wide development in tissue engineering, especially in the field of tendon regeneration.

The elements required to apply the electrospinning technique are:

- Polymer
- Solvent system (chemical compounds that allow polymers to dissolve. They must be volatile, so they can evaporate very quickly if put in contact with air, and they must be able to charge electrically)
- Syringe, to store the polymeric solution
- Pump, to extrude the polymeric solution from the syringe in a controlled manner
- Metallic needle
- DC high-voltage generator
- Metallic ground collector, which is intended to attract the nanofibers that are at higher potential.

The formation of nanofibers through electrospinning is based on the uniaxial stretching of a viscoelastic solution [70]. In the electrospinning process, a high voltage is used to create an electrically charged jet of polymer micro- or nanofibers by the syringe [71].

The solution is slowly pumped out of the needle tip, forming a spherical droplet, which has some surface tension. By connecting the droplet to the high-voltage power supply, its surface is covered with charges of the same sign. The electrical repulsion between the charges on the surface destabilizes the shape of the droplet. If the electrical repulsion exceeds the surface tension force, the droplet deforms and assumes a conical shape (Taylor cone), and a jet will emanate from the apex of the cone [72]. The repulsive forces cause the liquid jet to move toward the collector [25].

This movement causes the polymer chains in the solution to stretch and slide over each other, resulting in fibers with diameters in the nanoscale (Fig.9). The morphology of the electrospun fiber depends on the distance between the needle and the collector and also on the polymer solution. If the distance is small, large-diameter nanofibers are formed; if the distance increases, the diameter decreases [73–76]. The solvent system plays a key role to prevent the formation of undesirable beads [25].

The degree of volatility of the solvent is crucial to the electrospinning process. A solvent that is too volatile will cause the bead to dry at the needle tip, blocking the process. A solvent that is too low in volatility does not allow for adequate drying of the nanofiber jet, and the deposition of solvent-containing nanofibers on the collector can cause the formation of beaded nanofibers [77]. The conductivity and dipole moment of the solvents are also important [73,78].

The electrospinning process depends on three families of parameters:

- Solution parameters: solution concentration, polymer molecular weight, solution viscosity, solution conductivity, and solvent volatility.
- Process parameters: voltage, flow rate, needle/collector distance, collector shape, collector rotational speed, and needle diameter and structure.
- Environmental parameters: humidity and temperature.

By properly adjusting the combination of these parameters, the shape, cross-section, and orientation of the obtained nanofibers can be tuned [70–73,79].

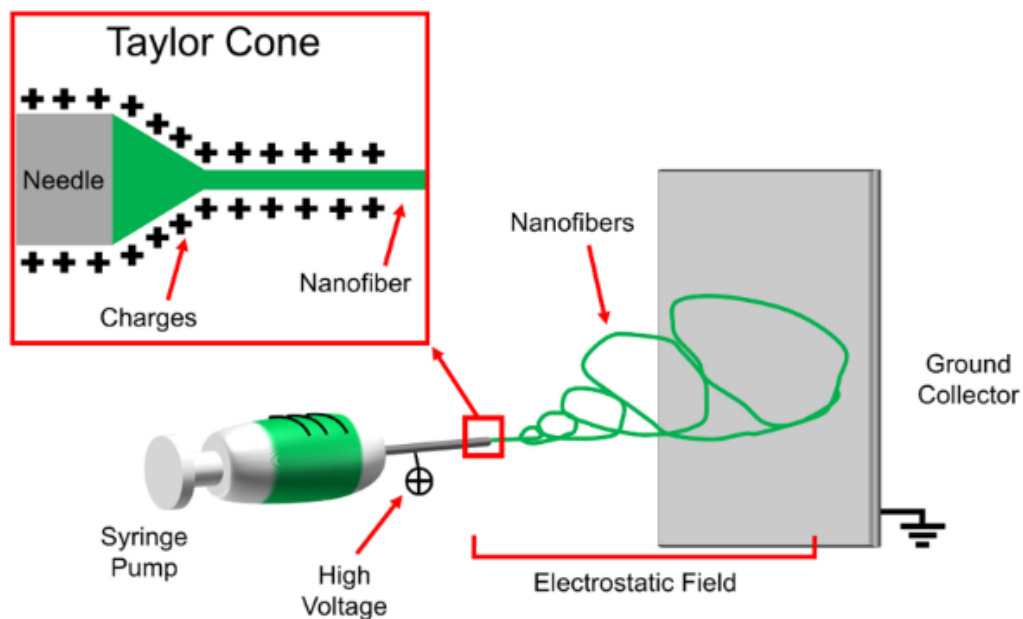


Fig.9 Electrospinning operating principle and Taylor cone formation [25].

Other key parameters to control the morphology and orientation of the nanofibers are the shape and movement of the ground collector. Using a flat metal plate (Fig. 10A), we obtain nanofibers with isotropic (random) orientation. The same orientation can be obtained using a drum collector rotating at a speed of less than 8m/s (Fig.10B). The obtained random mats are suitable to reproduce the structure of spongy bone or fibrocartilage, and also their porosity. By increasing the speed of the collector, the nanofibers align along the circumference of the drum, generating a structure with a unidirectional anisotropic orientation (Fig.10C).

The same configuration can be achieved with the gap collector (Fig.10D), which consists of two metal rods or bars, placed at ground potential, separated by a gap. The nanofibers align by being attracted to the ground potential of both collectors, filling the gap. This method only works if a very small gap, less than 100mm, is used. After removal of the anisotropic mat from the drum or gap collectors, shrinkage of the nanofibers can be observed, giving the uniaxial constructs the nonlinear mechanical properties and morphology typical of muscle and tendon structures [4,25].

Electrospinning appears to be a promising technique for tendon regeneration. This is due to its ability to obtain nanofibers with resorbable materials, achieving a morphology similar to that of the collagen fibrils that constitute these tissues. [80,81]. Electrospinning is also suitable to produce scaffolds that can reproduce the typical non-linear toe region, the ECM organization, and the biomechanical properties of tendons [81].

Replacing a classical metal collector with a liquid bath to collect the nanofibers is the method used in wet electrospinning (Fig.10E). This technique allows increase the pores of electrospun mats and remove residual charges from the surface. Another method used to obtain nanofiber mats deposited in specific directions is based on the deposition of specific patterns on the flat collector (lines or grids) (Fig.10F). Although aligned fibers enable mechanical properties closer to native ones than randomly arranged fibers, they are still unable to provide adequate yield and ultimate tensile strength [25].

Several techniques have been used to improve mechanical properties, such as co-electrospinning, in which two different polymers are electrospun simultaneously from two different syringes (Fig.10G). The two different fibers are then collected by the same collector forming a mixed fiber network. Another method used is multilayer electrospinning, in which different polymers are electrospun layer by layer on the same collector (Fig.10H) [25].

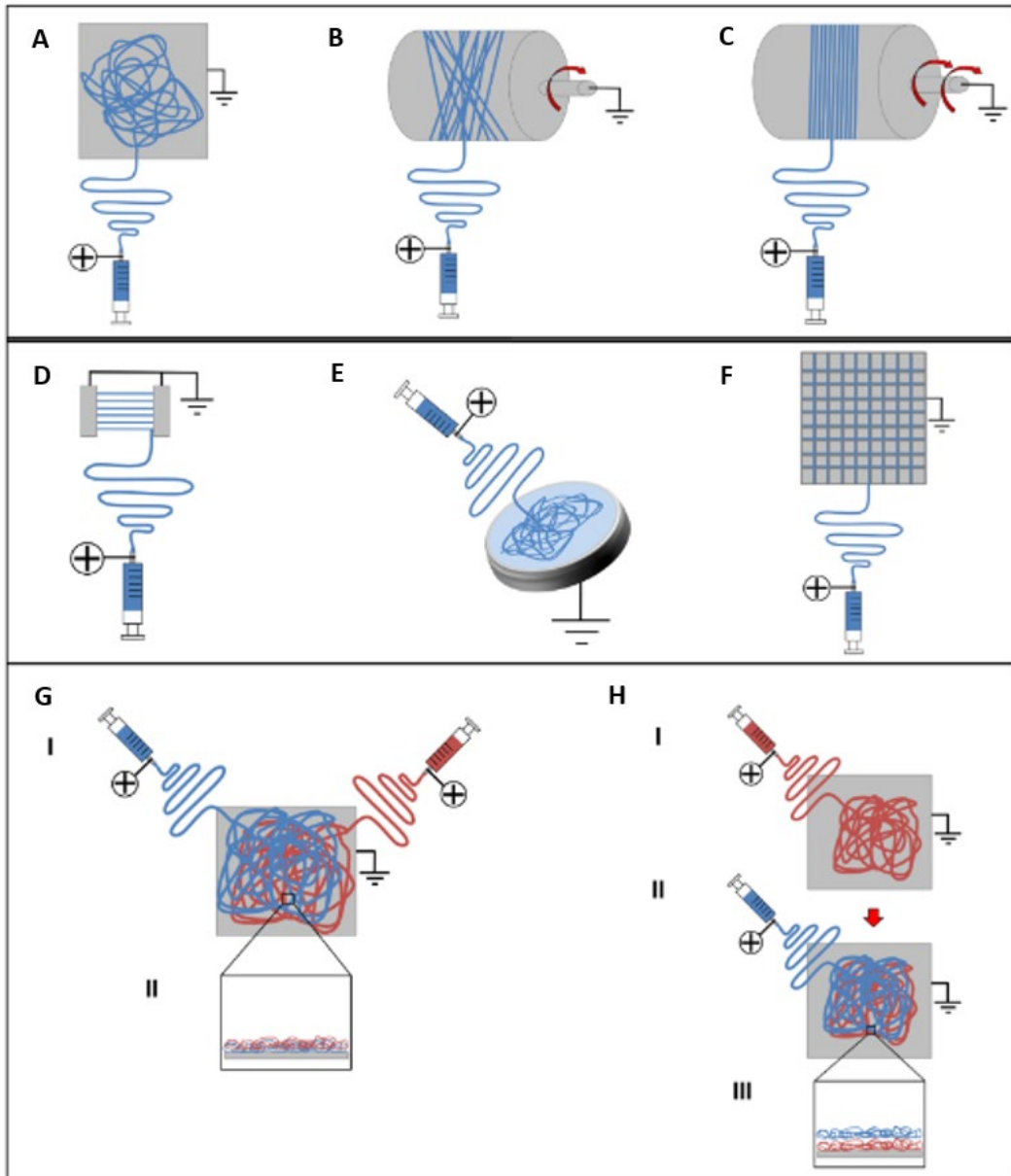


Fig.10 Different electrospinning setups to produce mats of nanofibers: (a) flat plate collector;(b) drum collector rotating at low speed, producing random nanofibers; (c) drum collector rotating at high speed, producing aligned nanofibers; (d) gap collector; (e) liquid bath collector; (f) flat plate collector with a grid pattern on the surface; (g) mixing electrospinning or co-electrospinning setup ((I)two syringes electrospun synchronously the solutions on a flat plate collector; and (II) section of the mat with the two different nanofibers mixed; and (h) multilayering electrospinning setup((I) one solution electrospins on a flat plate collector producing a random mat; (II) a second solution electrospins the previous random mat; and (III) section of the final mat shows two different layers of nanofibers overlapped) [25].

Specific electrospinning designs have been studied to develop gradients of random and aligned nanofibers or continuous regions with different materials. Among these specific techniques, there is the multilayer electrospinning, which consists of the production of the first mat of isotropic or anisotropic nanofibers and a further mat arranged on the previous one, obtained with a polymer solution equal to or different from the previous one. Co-electrospinning consists of the simultaneous electrospinning of two different solutions on a drum or flat collector, obtaining mats with two different types of nanofibers [10]. These two techniques are well suited to mimic the orientation gradient of MTJ. Since additive manufacturing (AM) is not able to reproduce the structure of biological tissues, while electrospinning has relevant limitations in simulating the mechanical behavior of the tissue, many research groups are working on the combination of electrospinning and AM technologies. To improve the biocompatibility and mechanical properties of nanofibers, blends of biomaterials can be combined with them. Drugs, growth factors, and nanoparticles are used to increase bioactivity and accelerate cell proliferation [10].

Regeneration of musculoskeletal junctions is one of the greatest challenges in tissue engineering. Several techniques have been used to try to improve this field and, among them, electrospinning seems to be the most promising. Over the years, different materials and designs have been used starting with simple mats and then taking on increasing complexity. Despite the encouraging results, several improvements are still needed regarding the multiscale morphology and mechanical properties of the scaffolds, as they are still inadequate for implantation in human patients [10]. A possible promising solution could be offered by improving the integration between AM, bioprinting, and electrospinning. This may pave the way for scaffolds that come closer and closer to mimicking native tissues.

Through the electrospinning technique, it is possible to obtain different types of structures, the most common are Yarn and Bundle types. One of the easiest ways to obtain a bundle is to electrospin a mat of nanofibers with a drum collector rotating (Fig.11A) at a peripheral  $\geq 8\text{m/s}$ . This allows to obtaining a mat with aligned nanofibers (when the peripheral speed is  $< 8\text{m/s}$  instead, random nanofibers are obtained). Then, the mat is cut into several bundles that are rolled up on themselves, obtaining nanofibers aligned along the axis called bundles. The yarn-type fibers (Fig.11B) are obtained using the "Funnel Collector", consisting of a metal cup rotating at a given speed set at zero potential. The nanofibers are deposited by attaching themselves with the tips to the sides of the cup creating a sort of drum skin. In the upper part of the collector is inserted a small filament that pierces the mat, the fibers are fixed on this filament which is then brought back with a rotating movement. In this way the fibers are transported twisting on themselves, thus obtaining the yarn fiber.

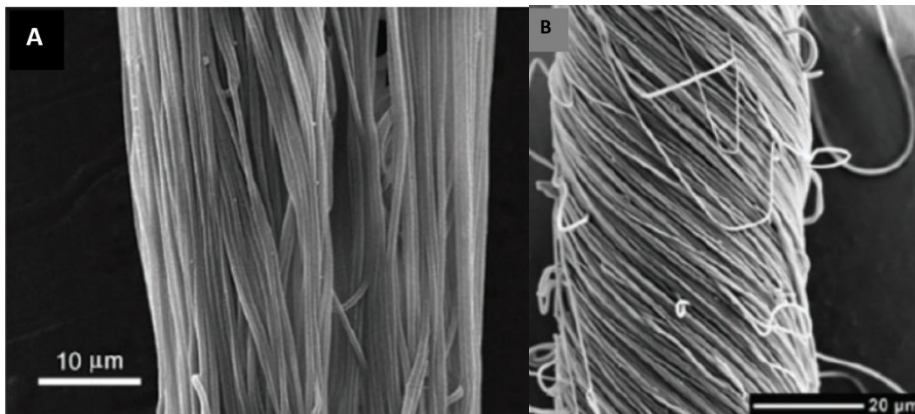


Fig. 11 A) SEM image of an aligned nanofiber bundle; B) SEM image of a twisted nanofiber yarn [82].

## 1.7 3D PRINTING

The human body has little capacity for regeneration. The options to date used to replace damaged tissue involve the use of grafts. This practice presents the difficulties described above, which is why regenerative medicine and tissue engineering are working on new techniques to solve the problem.

3D printing is a technology used in different fields, such as biomedical, but also industrial. It is a technological process that generates three-dimensional structures from artificial materials of different kinds.

This technology allows obtaining customizable constructs. The printer knows the project to be realized through software and can recreate the structure with a micrometric resolution.

3D printing (or additive manufacturing (AM)) is a technique for manufacturing objects with precise geometry, this technique uses computer-aided design (CAD). The 3D model designed in CAD software is converted to STL format, which is then broken down into 2D profiles. Each 2D layer of the model is glued to the previous layer on the build platform until the finished object is obtained [83].

3D printing technology seeks to fabricate tissue constructs that can mimic the structural and functional properties of native tissues. This technology is particularly useful for complex tissues such as those in the musculoskeletal system, which possess regional differences in cell types and mechanical properties. 3D printing can be used to finely tune the architecture and porosity of the scaffolds described earlier. The main AM technologies are selective laser sintering (SLS), stereolithography (SLA), fused deposition modeling (FDM), inkjet 3D printing (I3DP), and 3D bioprinting(3DBP). Elements to consider when choosing one of these technologies are accuracy, materials, time, and cost of manufacture [83].

I3DP is a non-contact reprographic technique that takes digital data from a computer representing an image or character and reproduces it onto a substrate using ink drops[84]. It uses a polymer in the form of a powder that initially sits on one shelf. There is then a roller that moves a layer of powder (the thickness of which depends on the resolution of the printer itself) to a second shelf. The printer head contains a curing resin, and this is positioned at the appropriate coordinates by the software and cures the polymer only where required in the x-y plane. After the first layer is finished the second shelf is lowered along the z-axis and the roller moves a new layer of polymer powder to repeat the process. In this way, the scaffold is formed layer by layer and at the end of the process, it will be necessary to remove the excess powder and finish it if necessary.

FDM is the most widely used 3D printing technology because it is inexpensive and simple to use. The polymer is used in a solid-state. In this technique, polymer filaments are extruded through nozzles heated to the polymer's melting temperature, which transforms the material into a semi-liquid phase. At this point, the semi-liquid material is selectively deposited on a printing platform layer by layer. The printer head moves in the x-y plane so that the first layer of the object can be formed. The plane on which we build the object, on the other hand, moves along the z-axis, allowing the process to build layer by layer. The problem with this technique is that it requires high printing temperatures, which cause degradation of the cells; it also has relatively low resolution. Another problem with this technique is that it requires support material if the object involves cavities, and this causes a lot of material waste [85].

SLS, on the other hand, is a technique that uses a laser to selectively polymerize certain coordinates of the polymer powder layer that is on the printing platform. During the printing process, the laser is guided to draw a specific pattern, once the first layer is finished, a roller distributes a new layer of powder on top of the previous one. The advantage of this technique is that it does not require the use of solvents and has a higher resolution due to the precision of the laser. The problem is that high temperatures are also required in this technique, making it very difficult to introduce the technique into the medical field. High temperatures can degrade cells and drugs, for this reason, SLS is used only in the field of tissue engineering and for drug-eluting devices in which the drug has been inserted after the printing process. The advantage is that this technique does not require the use of support material, reducing the waste material[83,85].

SLA uses a light source with a wavelength in the ultraviolet. The polymer is in the form of a liquid, enriched with a molecule that if hit at a certain wavelength makes the material polymerize (photopolymer). The light strikes the material at certain points to create the object, which is produced from top to bottom upside down. This type of printing allows for very high accuracy and requires little support material.

3D bioprinting is an emerging technology with various applications in creating functional tissue constructs to replace damaged tissues. During the bioprinting process, a solution of a biomaterial or a mixture of different biomaterials in the form of a hydrogel, called a bioink, is used to create tissue constructs. Bio inks can be formed from natural or synthetic biomaterial or a combination of the two (hybrids). This technique allows the fabrication of three-dimensional tissue constructs with programmed structures containing living cells. The process is accomplished by synchronizing the deposition of the bioink with the movement of the printing platform. In addition, the use of multi-head deposition systems allows the simultaneous or subsequent printing of multiple materials [86].

The main problem that all these techniques have in common is resolution. 3D printing does not have a resolution that reaches the nanoscale, this does not allow to obtain the nanofibers necessary to reproduce the tendon tissue, which is of fundamental importance to be able to regenerate the MTJ. That's why researchers are trying to develop new 3D printing techniques that can achieve better resolution, such as melt-electrowriting.

## **1.9 MATERIALS**

Using suitable materials in the production of scaffolds that must regenerate the tissue of the MTJ is of fundamental importance since the material used must reproduce the mechanical properties of the tissues that make up this tissue structure [25]. Typically, these scaffolds are made of two different types of materials, one that must best reproduce the tendon structure and the other that must best reproduce the muscle structure. Then, the two materials are made to interact to verify that they can regenerate the structure of the native interface.

The most used materials are polymers, which have mechanical properties similar to those of the native tissue, in particular, they have a good deformation capacity if subjected to mechanical stress. Both bioresorbable and non-bioresorbable polymers can be used, depending on the patient's condition. Bioresorbable polymers (natural or synthetic) are best suited for young patients or athletes, as they exhibit very rapid cellular and metabolic activity.

This allows the patient's tissue structure to develop to replace the support structure over time. In contrast, non-bioresorbable materials are indicated for older patients, as they exhibit less cellular activity and metabolic response. This is the main reason why the mechanical properties of tendons decrease with advancing age [25].

In the studies carried out, different types of materials have been used to regenerate tendon and muscle tissue, but also mixtures of polymers have been used to perform electrospinning and natural or synthetic nanoparticles or drugs to improve the properties of the polymers used.

**Table 4:** Materials

<b>Acronym</b>	<b>Extended name</b>	<b>Application</b>	<b>References</b>
PU	Polyurethane	Muscle side	[30]
PLLA	poly-L-lactic acid	Muscle side	[47]
PCL	Poly( $\epsilon$ -caprolactone)	Tendon side	[30,47,87]
Coll	Collagen	Whole scaffold	[88]

## **2 AIM OF THE THESIS**

The aim of this thesis is to investigate the methodologies known to date for biofabricating an injured MTJ. Injuries to the MTJ result in motor disabilities and pain and are difficult to fix. The difficulty in the biofabrication of this construct lies in the fact that it is an interface site between two very different tissues. By investigating the experimental techniques that are used to attempt to regenerate the MTJ, it will be possible to realize the advantages and disadvantages of each technique and evaluate which of them is the most promising. In addition, it is possible to mix techniques and use several of them to obtain better constructs that more closely resemble the native one. To date, none of the reported studies have succeeded in obtaining constructs that can be used definitively. But many of them have obtained promising structures from both mechanical and morphological perspectives.

In addition, through the analysis of the studies performed, it was also possible to compare the cells and polymeric materials used to create the scaffolds. Many studies have succeeded in obtaining good cell proliferation, but in some cases, the mechanical properties do not reach those expected.

Although much research has been done to regenerate tendon and muscle tissue separately, a lot needs to be done to regenerate their interface. It is very important to obtain constructs that can replace injured MTJ, as it breaks down very often. The cause of frequent MTJ injury is that there is a high concentration of tension at this interface. This makes the MTJ among the most injury-prone areas in older people and young athletes.

The expectation for the future is to be able to generate constructs that can effectively replace injured MTJs. This would result in a huge step forward for modern tissue engineering.

### **3 METHODS OF THE RESEARCH STRATEGY**

The research was conducted systematically, using databases such as PubMed and Google Scholar. The articles used are located in a temporal range from 1973 and reach up to 2022. Many of the relevant articles were found through citation checking of individual articles. Only the articles relevant to this thesis were cited, while the other articles analyzed were not included.

The following strings were used to organize the different sections:

- For the introduction the most relevant articles concerning the following keywords were selected: Myotendinous junction, MTJ, MTJ regeneration, tissue engineering, tendon-muscle interface, melt electro-writing, electrospinning for MTJ regeneration, 3D printing, 3D bioprinting, melt electro-writing for MTJ regeneration, mechanical properties of muscle tissue, tendon tissue, hierarchical organization of muscle, mechanical properties of tendons, tendon injuries, MTJ injuries in sport, MTJ injuries, mechanical properties of MTJ, the structure of MTJ, scaffold for MTJ regeneration.
- For the “Aim of the thesis” the most relevant articles concerning the following keywords were selected: 3D printing for MTJ regeneration, scaffold for MTJ regeneration, MTJ regeneration, biofabrication for MTJ, additive manufacturing for MTJ regeneration, electrospinning for MTJ regeneration, graded scaffolds for MTJ regeneration, magneto-mechanical actuation for MTJ regeneration.

The impact factor of the journals from which the articles were taken ranged from 1.8 to 54.908.

## **4 RESULTS OF THE LITERATURE SEARCH**

The search for the following articles was done in such a way as to subdivide the types of scaffolds obtained to regenerate MTJ based on the technique used to create these scaffolds. First, experimental articles related to MTJ regeneration using electrospinning were searched. Next, a search was conducted on scaffolds obtained by 3D printing and finally a search was conducted on articles that used in vitro engineered constructs.

In the following section, the individual articles have been described in detail, so that we can compare the scaffolds obtained and understand which of these techniques is to be considered the most promising.

### **4.1 ELECTROSPINNING**

Studies performed for MTJ repair include one performed by Ladd et Al. (2011) [47], in which electrospinning was used to produce a scaffold to improve MTJ repair. In this study, random nanofiber membranes were obtained by co-electrospinning a PLLA/Col and a PCL/Col solution on a drum collector. PLLA was chosen due to its known biocompatibility, biodegradability, and relatively high stiffness. PCL was also chosen for its known biocompatibility, and biodegradability, but additionally because of its lower stiffness. Both polymers were blended with collagen as this improves cell attachment. The solutions were then simultaneously electrospun onto opposite ends of a cylindrical mandrel using a high voltage power supply at a potential of 20 kV. This resulted in 3 different regions, the first one consisting of PLLA the second one consisting of PCL, and the third region being an overlap of the previous two regions (Fig.12A). Crosslinking with glutaraldehyde vapor was performed to increase the mechanical integrity of the scaffolds and to prevent collagen from dissolving in water. Methyl blue dye was added to PLLA to visualize the dual scaffolding system.

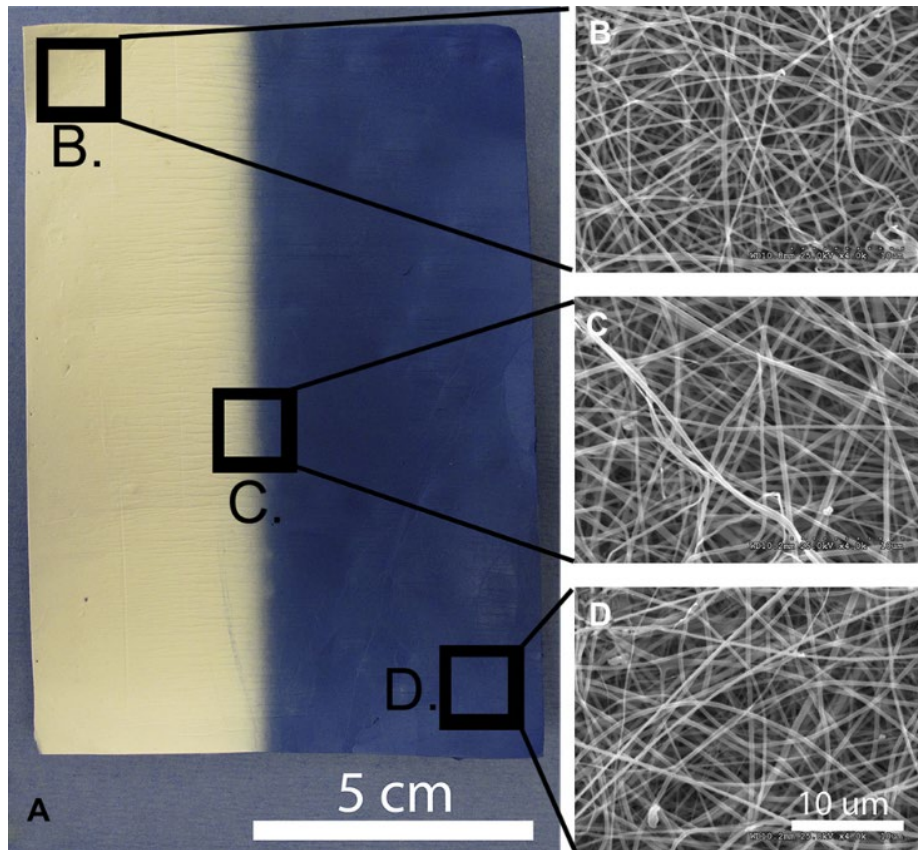


Fig.12 Gross picture and SEM images of a scaffold. (A) Image showing the three regions of the scaffold: PCL side, center, and PLLA side with the methylene blue dye in it. (B, C, D) SEM images from different regions of a scaffold showing fiber morphology and diameter (all images 4K). (B) PCL side, (C) Center, (D) PLLA side. Fibers showed rounded, nanoscale morphology. The PLLA side had smaller fiber diameters by approximately 100 nm, but there was no statistical difference between the fiber diameters of the different regions (n=6 for SEM) [47].

The mechanical tests performed showed that the created scaffolds had the following mechanical properties: Young Modulus equal to  $7.3 \pm 2.1$  MPa, tensile stress equal to  $0.5 \pm 0.2$  MPa, and ultimate strain equal to  $18.5 \pm 8.2\%$ . The values obtained are higher than those of native MTJ, which instead has a Young Modulus of  $0.3 \pm 0.1$  MPa, tensile at break of  $0.1 \pm 0.01$  MPa, and failure stress of  $122.4 \pm 19.9\%$ . Moreover, the polymer fiber in this scaffold was random, which was proven unsuitable for tendon regeneration compared to well-aligned fibers (Fig.12B-D).

**Table 5:** Mechanical properties of different regions of the scaffold compared to muscle, tendon, and native MTJ tissue. E=Young Modulus; UTS=ultimate tensile strength; SAF=strain at failure [47].

	<b>E (MPa)</b>	<b>UTS (MPa)</b>	<b>SAF (MPa)</b>
<b>PCL side</b>	4.490 ( $\pm$ 1.604)	1.069 ( $\pm$ 0.2713)	130.4 ( $\pm$ 44.56)
<b>Center</b>	20.06 ( $\pm$ 7.773)	2.384 ( $\pm$ 0.5987)	42.79 ( $\pm$ 17.75)
<b>PLLA side</b>	27.62 ( $\pm$ 6.063)	3.741 ( $\pm$ 0.8486)	35.33 ( $\pm$ 8.964)
<b>Whole scaffold</b>	7.339 ( $\pm$ 2.131)	0.5058 ( $\pm$ 0.2130)	18.49 ( $\pm$ 8.210)
<b>Native MTJ</b>	0.2789 ( $\pm$ 0.1509)	0.1478( $\pm$ 0.01631)	122.4 ( $\pm$ 19.18)
<b>Muscle</b>	0.005-2.8	-	-
<b>Tendon</b>	500-1850	52-120	5-16%

There are several problems with this research. First, the fibers obtained by electrospinning are organized in a random, non-aligned fashion. This is a major flaw since in the native structure of MTJs the fibers turn out to be strongly aligned, providing an anisotropic behavior that gives them better mechanical properties along the alignment axis. Another problem encountered is the choice of the researchers not to use a dynamic culture (using a bioreactor), which could have improved the mechanical properties of the scaffold by allowing the fibroblasts to achieve a more elongated, noncircumferential configuration as in the image. Unlike myoblasts, which tend to take on a tapered, elongated shape even without undergoing mechanical characterization, fibroblasts require the dynamic culture to take on a native-like configuration. Despite this, we can state that the chosen materials result to have a mechanical behavior quite similar to the native structures, although with different ranges (Fig.13).

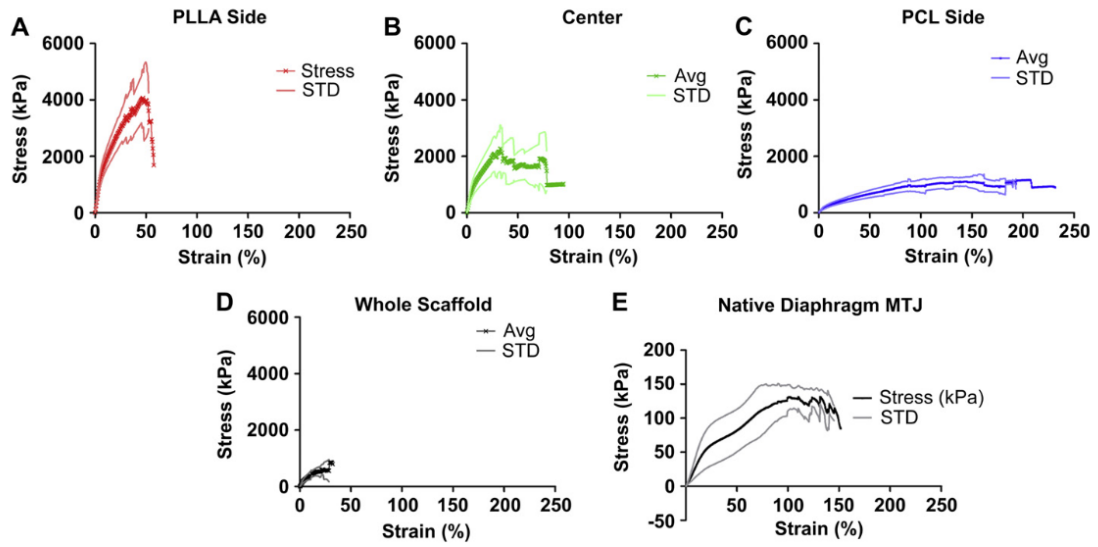


Fig.13 Average stress-strain curves from tensile testing to failure. (A) The PLLA side (n=9) shows a high modulus and UTS with low strain at failure. (B) The center (n=9) shows a modulus and UTS in between the PLLA side and PCL side and a more variable strain at failure. (C) The PCL side (n=9) exhibits a low modulus and UTS with a very high strain at failure. (D) The whole scaffold (n=10) exhibits its own set of properties as it is a composite. (E) Native diaphragm muscle-tendon junction. Note that the scale here is different from (A-D). [47].

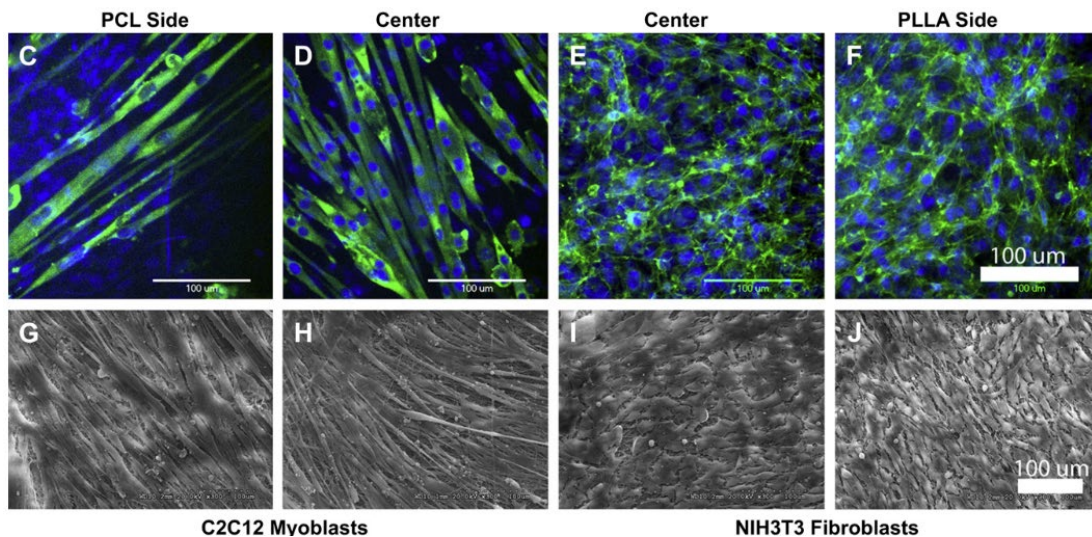


Fig.14 (A, B) MTS assays demonstrating cytocompatibility of the scaffold regions. Data are expressed as percent viability which is the average absorbance normalized to the average absorbance of tissue culture control. The values are the average of 3 experiments done with 6 replicates in each group for a total replicate number of  $n=18$ . (A) The scaffolds show no statistical difference in cell viability at 3 days and at 7 days there was a slight increase in percent viability in the scaffold groups, but this difference is likely due to experimental error. (B). For the fibroblasts, at both 3 and 7 days, no differences were found in viability between the scaffolds and tissue culture controls. (C-J) Confocal (C-F, all images 200) and SEM (G-J, all images 300) images of scaffolds seeded with C2C12 myoblasts or NIH3T3 fibroblasts. (C-D, G-H) All three regions were able to accommodate C2C12 attachment and differentiation into myotubes (green=MF20, a myosin heavy chain marker, blue=ToPro nuclear stain). Only the PCL side and center are shown. (E, F, I, J) Additionally, all three regions were able to accommodate fibroblast attachment (green=phalloidin, blue=ToPro nuclear stain). Only the Center and PLLA sides are shown. All cell seeding experiments were done in triplicate with 3 replicates per region for confocal and SEM for a total of  $n=9$  for each region for both confocal (except for PCL side on confocal,  $n=8$ ) and SEM analysis. [47].

Another study was performed by Kishan et Al. in 2017 [89] in which the techniques of in-line blending and air-gap electrospinning are combined. These techniques were used to allow fiber alignment in the direction of the scaffold gradient. A custom collector with synced rotation permitted fiber collection with uniform mesh thickness and periodic copper wires were used to induce fiber alignment. A gradient composition scaffold was used, with and without fiber alignment. A fluorescent dye was used to characterize the compositional gradient of the mesh. As expected, the mesh with aligned fibers induced a corresponding alignment of cells in static culture.

These techniques allow the fabrication of scaffolds with macromolecular gradients in the direction of alignment, proving to be very valuable in the engineering of interface tissues, such as MTJ.

To evaluate the combination of in-line blending and air-gap electrospinning as a means of fabricating macromolecular gradients in aligned electrospun structures, high and low hard segment Biodegradable polyurethane ureas (BPURs) were used. The effect on cellular orientation was evaluated by culturing mesenchymal stem cells.

Two syringe pumps were connected in parallel through a y-connector, from the two pumps two different BUPR solutions were extruded, one with low hard segment content and one with high hard segment content (Fig.15). The first solution had a flow rate that ranged from 0.3 to 0mL/hr, while the second ranged from 0 to 0.3mL/hr. In this way, the first electrospun fibers were mainly from the first solution, while the last was from the second solution.

The mixing head was then connected to a needle with a positive voltage, while the negatively charged collector was placed 20cm away. Two meshes were obtained, one with aligned fibers and one with random fibers.

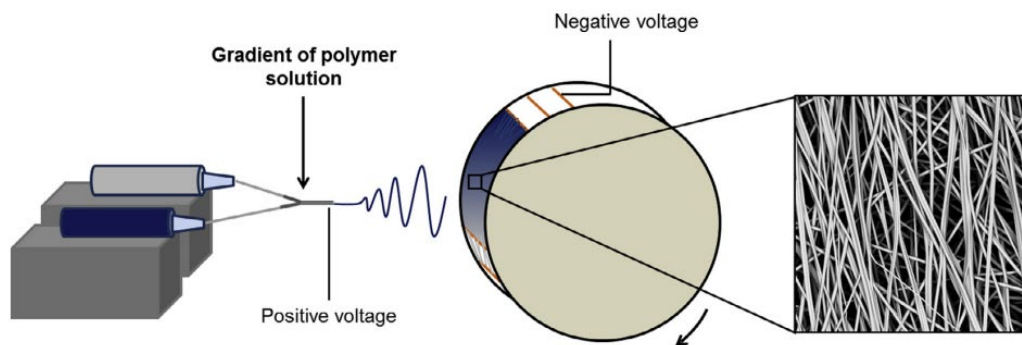


Fig.15 Schematic of the electrospinning set-up [89].

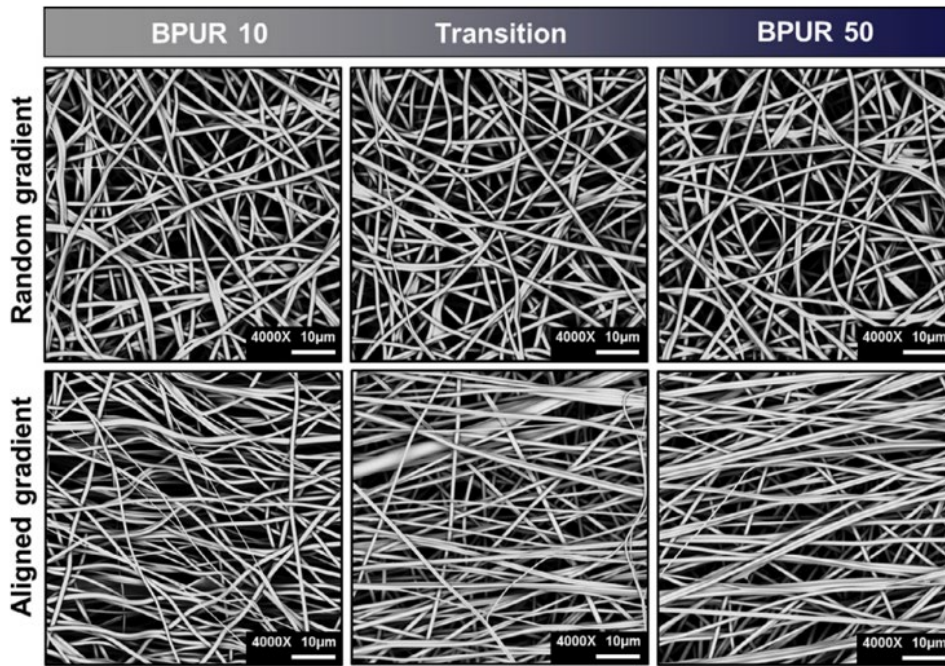


Fig. 16 SEMs of each region in random and aligned gradient electrospun scaffolds [65].

Next, a tensile test was performed for both types of meshes. They were sectioned into three regions, one with BPUR 10, one transition region, and one with BPUR 50. The test was performed using a testing machine with a 100N load cell. Thanks to the stress-strain curves, it was possible to derive Young Modulus, failure stress and strain.

Regarding the cells used (hMSCs), it has been noticed that their adhesion remains unchanged in the three regions and also between the two types of structures (random and aligned), the only difference is in their distribution, which results to be aligned to the fibers in the case of the aligned configuration.

Regarding the mechanical properties, we can say that they vary a lot from region to region, in both the structures studied. The region with BPUR 10 presented the lowest Young Modulus and the highest failure strain, while the region with BPUR 50 presented the highest Young Modulus but the lowest failure strain. In contrast, the interface region exhibited intermediate mechanical properties. This shows that the technique used resulted in a structure with gradual mechanical properties.

The aligned structure exhibited a modulus between 0.19MPa and 2.39MPa, while the random structure exhibited a modulus between 0.28MPa and 2.13MPa.

Overall, this technique provides greater control over the fabrication of heterogeneous scaffolds that better mimic the complexity of native tissue interfaces.

The development of biomimetic scaffolds that can also be used as bio-integrated actuators would not only facilitate mechanical stimulation of the engineered tissue but also continue to provide the mechanical stimuli *in vivo* after transplantation, increasing the regenerative potential of the system. Magnetic fields can be used as exogenous mechanical triggers of magnetic scaffolds to exert forces on seeded cells without directly affecting membrane receptors and ion channels. By using polymeric compounds incorporating magnetic particles, deflections of the substrate are caused which generates transient physical forces that are transferred to the cells by promoting mechanotransduction mechanisms that drive the cells toward the desired behavior.

In the study performed by Tomas et Al. in 2019 [90], a 3D magnetic responsive fibrous scaffold was generated that mimics the native tendon architecture and its mechanical behavior. This scaffold aims to create an artificial niche capable of magnetomechanically stimulating cells, both *in vitro* and *in vivo*.

To obtain this scaffold, PCL was electrospun in an aligned and continuous manner and MNPs (magnetic nanoparticles) of iron oxide were inserted to confer mechanical reinforcement and magnetic reactivity to the construct. The biological performance and functionality of hASCs (human adipose-derived stem cells) in the presence and absence of magnetic stimuli were then evaluated, to verify the consequences, especially regarding the tenogenic differentiation of the stem cells used. PCL fibers were also electrospun in solution with DT-NP in different proportions to evaluate the effects.

The morphology and size of the nanoparticles used were evaluated by atomic force microscopy (AFM), scanning electron microscopy (SEM), and transmission electron microscopy (STEM).

PCL nanofibers produced by electrospinning were twisted to obtain Yarn fibers and then woven into 3D scaffolds to obtain the actual scaffold. The mechanical properties of the structure formed by PCL and DT-NP were evaluated using a 1kN load cell testing machine. These mechanical tests showed that the mechanical properties of PCL/DT-NP5 fibers improved compared to those of PCL alone, the Young Modulus increased by 78% to  $21.55 \pm 4.91$  MPa, and the yield strength increased by 58% to  $2.22 \pm 0.30$  MPa, and the tensile strength increased by 62% to  $4.70 \pm 0.53$  MPa. Young Modulus and tensile strength of PCL/DT-NP5 constructs are within the range of native tendon tensile properties (20-1200MPa and 5-100MPa), but only in the lower range. The yield stress is adequate for tendon applications since the physiological range of native tissue is 4% strain. The stress-strain curves have a trend that reflects the properties of the native tendon.

We can say that PCL/DT-NP5 nanocomposites showed the highest mechanical properties while maintaining a fibrous structure mimicking the tendon.

For this study, the culture of hASCs with and without mechanical stimulation persisted for 21 days. The results showed a greatly increased cellular metabolic activity between day 11 and day 21, whereas no differences in this regard were noted between the culture with magnetic stimulation and that without magnetic stimulation, suggesting that this does not affect these cellular characteristics. In both cultures, cell morphology shows development aligned along the direction of the yarn fibers. The cells tend to assume an elongated configuration typical of tenocytes. The main difference between the static culture and the one subjected to remote mechanical characterization by magnetic properties is noted in the improved uniaxial alignment of the cells and elongation along the longitudinal direction of the fibers.

Cells can adapt their behaviors in terms of proliferation, differentiation, or maintenance of tissue phenotype by sensing external mechanical stimulations. External physical signals such as deformation of the culture substrate can be examined through the behavior of YAP/TAZs. YAP/TAZs are predominantly cytoplasmic, but when activated they travel forward-backward from the cytoplasm to the nucleus, where they regulate gene expression. The expression of YAP/TAZs in cultured hASCs after 11 and 21 days was evaluated to test whether magnetic scaffolds can provide mechanical stimuli to seeded cells, with remote magnetic actuation, acting as a promoter of tenogenic commitment. Following the application of a 300 mT magnetic field, immunofluorescence images were obtained showing predominant YAP/TAZ expression. The constructs were able to induce YAP/TAZ activation under both stimulated and unstimulated conditions, this demonstrates that their aligned topography is sufficient to induce this effect. The nuclear and cytoplasmic YAP/TAZ ratio in cells stimulated at day 11 is higher than that of cells cultured in static culture, this suggests that the mechanical loading signals were transmitted effectively. In contrast, on day 21, immunofluorescence images showed predominantly cytoplasmic YAP/TAZ, due to both decreased proliferation and cell crowding. We can, therefore, say that the magnetic-mechanical stimulation of cells was able to activate YAP/TAZ early suggesting effective transmission of the mechanical stimulus.

This study demonstrated that remote magneto-mechanical stimulation can drive mechanisms of mechanotransduction and tenogenic differentiation of hASCs and appears to have a positive impact on the expression of anti-inflammatory and healing gene markers. These effects may reduce tissue scarring at the site of injury during healing and improve the potential for strategies in the regeneration of engineered tendon tissue. Although this study focuses on the tendons, I believe that the same principle could be used on engineered constructs of the MTJ.

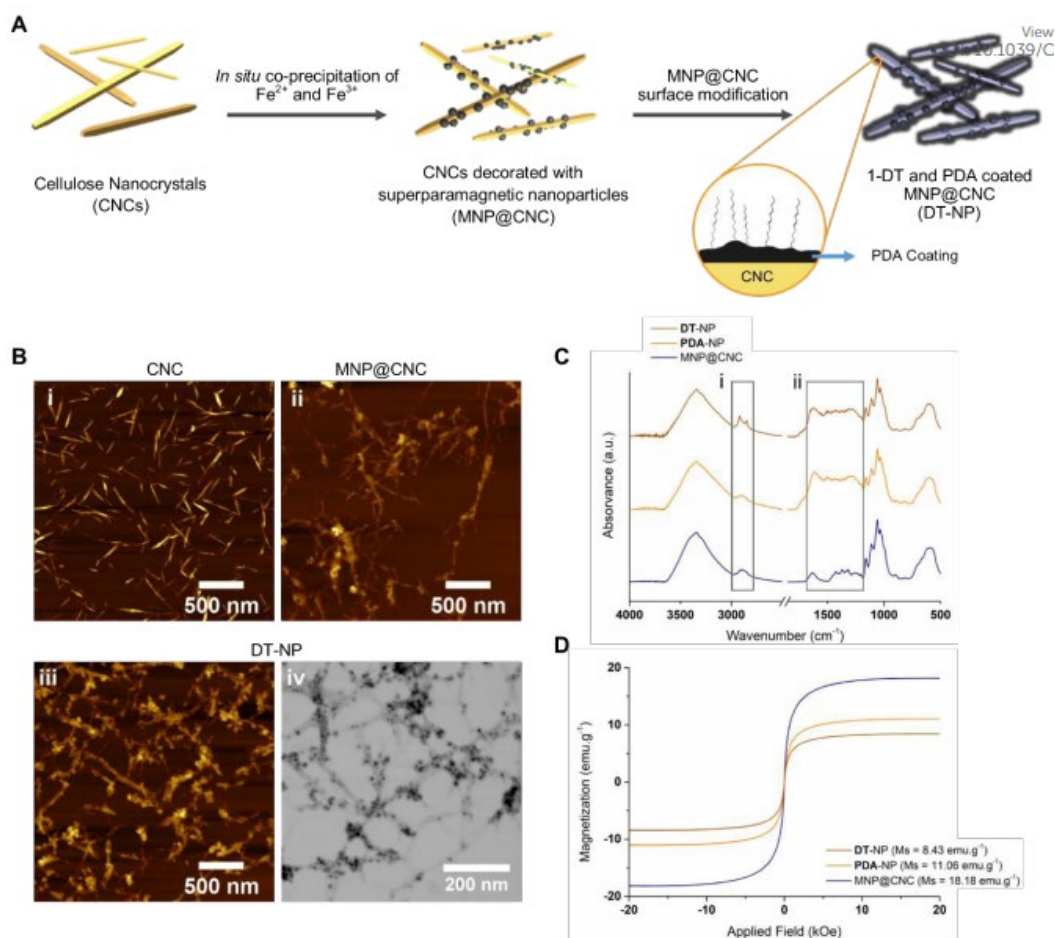


Fig.17 Production and characterization of the hybrid magnetic nanoparticles. A) Schematic illustrating the main steps involved in the production process. B) AFM images of CNCs (i), MNP@CNCs (ii) and of DT-NP (iii); STEM image of DT-NP (iv). C) FTIR spectra of MNP@CNC, PDA-NP, and DT-NP. Gray squares (i, ii) represent regions of the spectra in which characteristic pics of the different species can be identified. D) Magnetic hysteresis curves of MNP@CNC, PDA-NP, and DT-NP. Magnetization of saturation ( $M_s$ ) of each sample is shown next to the respective label.

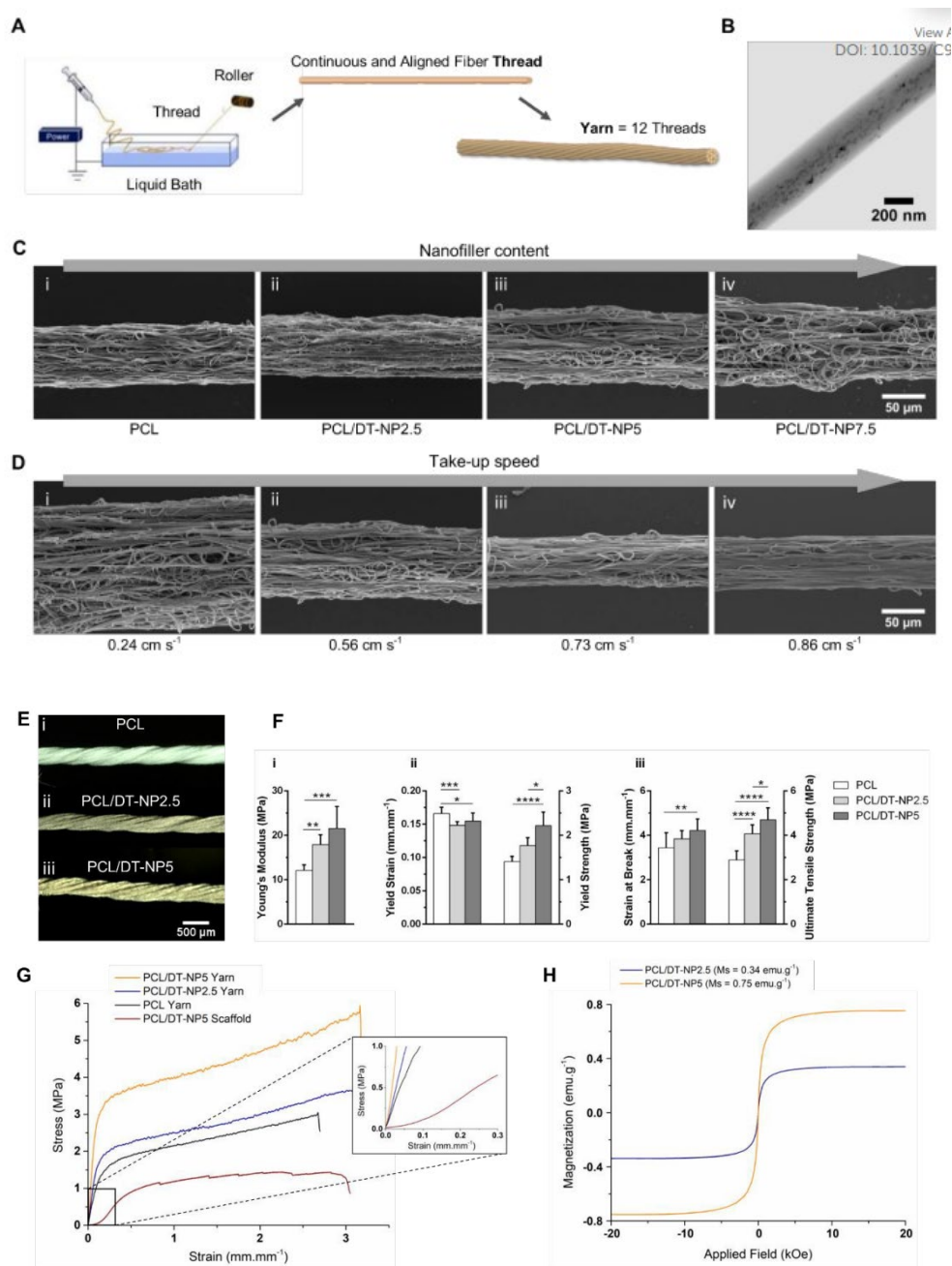


Fig.18 Fabrication and characterization of continuous and aligned electrospun fiber treats and yarns. A) Schematic illustrating the main steps involved in the fabrication of these fibrous constructions from the electrospinning set-up to the yarns. B) STEM image showing the dispersion of hybrid magnetic nanoparticles within PCL/DT-NP2.5 fibers. C) SEM images of PCL threads fabricated with different nanofiller content (0-7.5 wt.%) under the same spinning conditions. D) SEM images of PCL/DT-NP5 threads fabricated with increased take-up speed (0.24-0.86 cm/s). E) Optical microscope images of the yarns. F) Mechanical properties of electrospun yarns of increasing nanofiller content ( $*p \leq 0.05$   $**p \leq 0.01$   $***p \leq 0.001$   $****p \leq 0.0001$ ). G) Representative stress-strain curves of the fabricated yarns and 3-D scaffolds with an inset showing the behavior at low strains. H) Hysteresis curves of PCL/DT-NP2.5 and PCL/DT-NP5 yarns. Magnetization of saturations ( $M_s$ ) of each sample is shown next to the respective label.

Graded nanofibrous scaffolds were developed to reproduce the spatial distribution of interface properties in the study conducted by Hugenberg et Al. (2022) [87]. Graded scaffolds were created using previously described electrospinning. A solution of PCL in a chloroform-tomethanol solvent extruded from a syringe by applying a field of 18keV and collected on a rotating spindle with a rotational speed of 2000 rpm was used to obtain aligned nanofibers. To create scaffolds with spatially graded properties, a seven-layer design was used; the different layers were separated using paper strips placed over the spindle during deposition to avoid fiber accumulation in some layers (masking strips) (Fig.19). These masking strips were not directly in contact with the samples, so their removal did not affect the scaffold. The thickness of the nanofibers ranges from 200nm to 425nm. At the end of electrospinning, the multilayer mats were removed from the mandrel and cut into test rectangles, obtained so that the fibers were aligned along the axis of the specimen and the masked regions were centered within the length of the specimen, so that the specimens were more yielding in the center and stiffer at the ends. To subject them to tensile testing, the thickness of the specimens was evaluated using a metallurgical microscope.

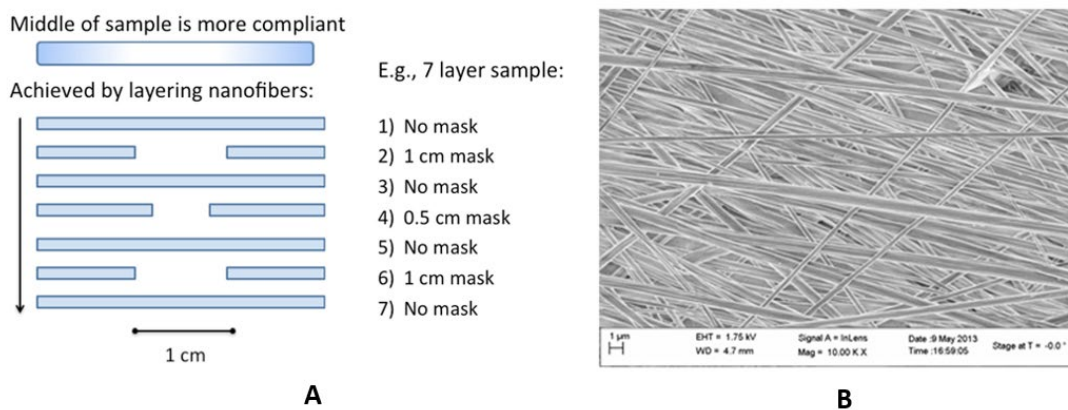


Fig.19 A) Schematic of seven-layered spatially graded scaffold design, and B) SEM demonstrating the specimen-aligned nanofiber topography [87].

The specimens were subjected to a uniaxial tensile test with a testing machine equipped with a 100N load cell. The specimen was stretched to failure at a constant rate of 0.2mm/s per second, and the displacement and time were recorded at a frequency of 50Hz. A stress-strain curve was obtained (Fig.20).

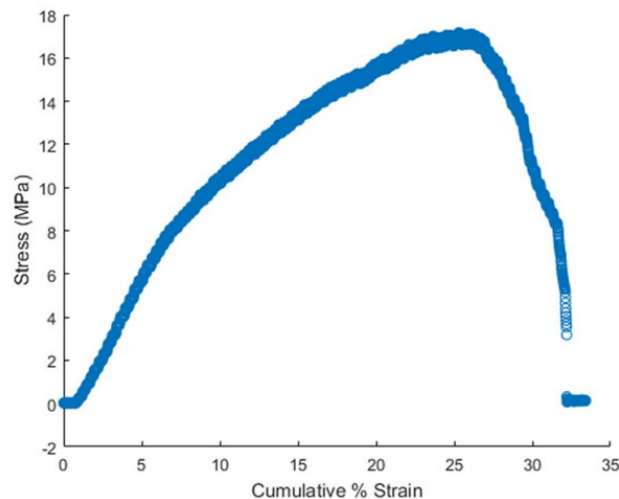


Fig.20 Representative stress-strain curve of a spatially graded electrospun PCL fiber mat subjected to constant rate elongation to failure, exhibiting bilinear behavior. This curve displays engineering strain for one sample [87].

The specimens exhibited a bilinear mechanical response characteristic in their strain stress curves, as displacements in the initial linear region of the specimens were analyzed. Due to a slight misalignment of the fibers concerning the specimen axis, the tensile test will see three modes of deformation as a result. The first mode sees the fibers reorient along the stretch axis causing an overall counterclockwise rotation, this corresponds to elongation along the axial direction. The second mode corresponds to lateral narrowing, which represents some form of rotation, but its contribution is three orders of magnitude less than the first mode. The third mode consists of random motions, composed mainly of noise. To remove noise from the data, PCA (principal component analysis) was used, and an inverse elasticity algorithm was applied to infer the spatial distribution of the Young Modulus of each sample. The spatial distributions of the Young Modulus are indeed gradual, this technique has not been applied specifically to regenerate the MTJ, but it could be a plausible solution to reproduce a gradual structure.

Type I collagen fibers provide a physiological and mechanoactive environment to coordinate cellular activity. Since collagen is biocompatible, biodegradable, and shows low immunogenicity it is used in tissue engineering techniques, being processed by electrospinning or wet spinning. In wet spinning, it is first dissolved in a suitable solvent and fiber formation occurs as soon as the solution is extruded into a coagulation bath [88], coagulation can occur by neutralization, dehydration, or ion exchange. This type of technique requires additional chemical cross-linking, such as glutaraldehyde, since the solvent that is used often breaks the weak bonds of the tropocollagen molecule, depleting the mechanical properties of this element. Cross-linking agents must be removed before collagen fibers are used, as they are found to have a cytotoxic effect. In the study conducted by Koeck et Al. (2022) [88] a blend of collagen type, I/III was processed into continuous non-crosslinked fibers with good mechanical properties. Scaffolds were developed to guide the blend into alignment, differentiation, and formation of organized myofibers (Fig.21). This construct was applied to a co-culture of myoblasts and fibroblasts to understand its application to MTJ.

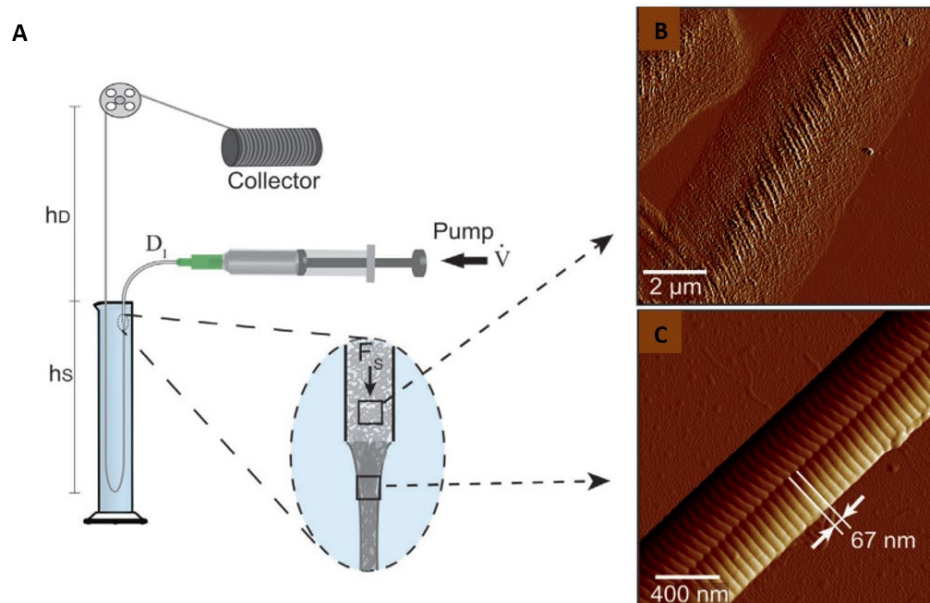


Fig.21 A) Schematic representation of the wet-spinning setup. The collagen solution is extruded into a coagulation bath through a needle connected to a syringe pump. Shear forces and a pH shift result in an alignment of the protein chains and fiber formation (close-up). To prolong the exposure time in the coagulation bath, the fibers were spun in a graded cylinder of a specific height to achieve stable fiber formation and enable rolling-up. The distance between the coagulation bath and the guide pulley and the cylinder height was adjusted in accordance with the needle diameter. AFM scans (amplitude representations) of the collagen structures in B) acidic spinning dope and C) in the alkalic coagulation bath. [88].

Continuous collagen fibers were wet spun, while collagen I/III fibers were dissolved in hydrochloric acid and spun in a coagulation bath containing ammonium hydroxide and acetone. In the stress-strain curves, dry fibers showed a linear elastic region from 0% to 2% strain, followed by viscoelastic strain up to the breaking point, corresponding to 16% strain. Wet spun fibers showed a toe region from 0% to 5%, followed by an elastic region up to failure. Toughness and tensile strength did not change if the solvent changed, while the Young Modulus of the hydrochloric acid-spun fibers ( $5106 \pm 447$  MPa) was higher than that of the acetic acid-spun fibers ( $4089 \pm 472$  MPa). Wet spun fibers exhibit lower tensile strength, lower toughness, and lower Young Modulus, but higher deformation than dry fibers. The data obtained show that it was possible to obtain collagen fibers without any cross-linking, while still maintaining good mechanical properties (Fig.22).

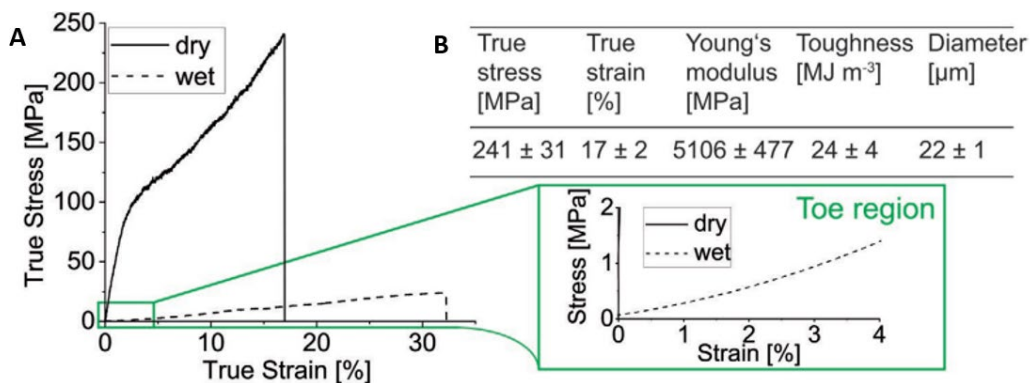


Fig.22 Mechanical and morphological properties of wet spun collagen fibers. A) Representative stress-strain curve of a dry and wet collagen fiber. The inset shows the toe region observed in the case of wet fibers (green box). B) Mechanical properties of wet-spun collagen fibers (n= 10). 10 mg mL<sup>-1</sup> dissolved in 10 mm HCl before extrusion into a coagulation bath. [88].

Cell viability and cell adhesion have been evaluated through different types of tests, including almarBlue and fluorescence images (Fig.23). These tests demonstrated excellent cell viability and good proliferation, but above all perfect cell adhesion, which resulted in the development of an aligned morphology along the fiber axis. Most C2C12 myoblasts fused to form multinucleated myotubes along the collagen fiber axis. The generated muscle fiber bundles showed highly organized cellular organization, capable of contracting upon electrical stimulation.

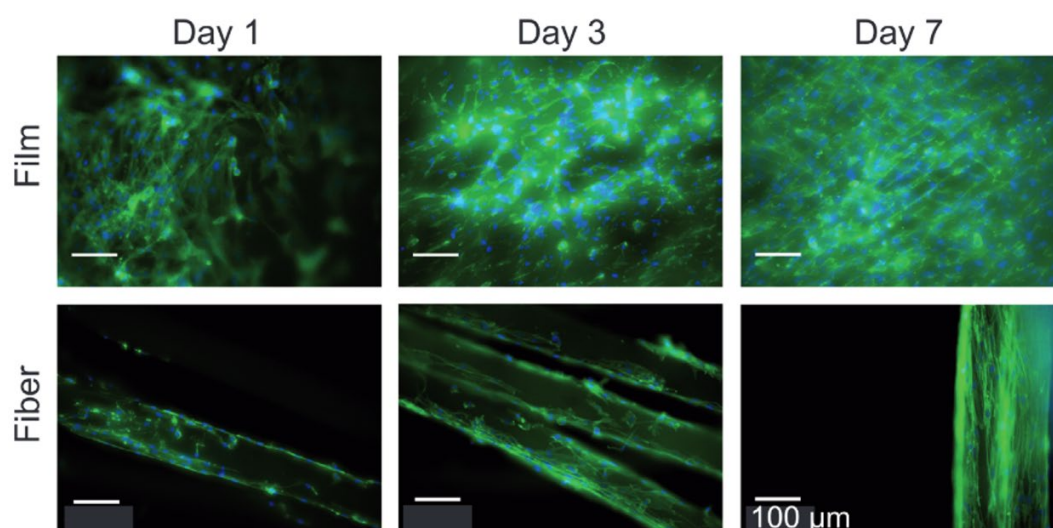


Fig.23 Cell culture analysis of C2C12 myoblasts on collagen films, or wet spun collagen fibers. Cell alignment: Fluorescence images of 4',6-diamidino-2-phenylindole dihydrochloride (DAPI) (blue, nuclei)- and phalloidin (green, actin filaments)-stained cells after 1, 3, and 7 days of cultivation. [88].

Using some 3D printing techniques, textile engineering techniques were applied to collagen fibers to obtain highly organized structures (Fig.24). Among the obtained structures, flat ones were used to obtaining an engineered construct to be applied to MTJ regeneration.

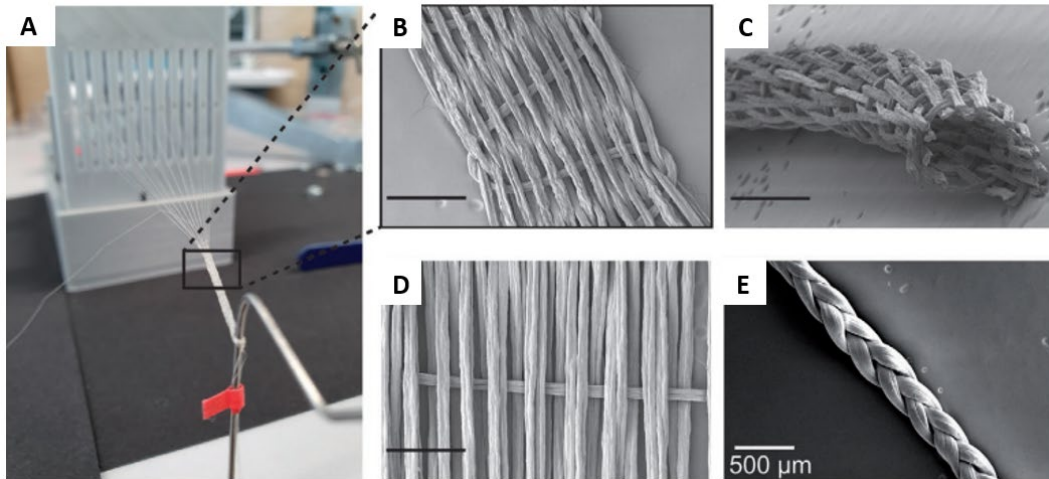


Fig.24 Collagen fiber processing. A) Photograph of the tape loom used to fabricate flat and tubular woven collagen structures. SEM images of structures with various morphological features were fabricated using wet spun collagen fibers. Image of collagen fibers woven in a B) flat and C) tubular structure fabricated using a tape loom. D) Image of a flat structure created by weaving collagen fibers using a frame. E) Image of a braided structure using three single collagen fibers. Scale bars are 500  $\mu\text{m}$ . [88].

Using a co-culture of C2C12 and NIH-3T3 on flat structures made of wet-spun collagen fibers, a model of MTJ could be developed. Initially, C2C12 was labeled with a green cell tracker and NIH-3T3 with red. Cell adhesion and proliferation were successful for both cell types. Once moved into the differentiation medium, long, aligned myotubes were formed. The experiment was then conducted again without the use of trackers. On day 7, the cells were stained with  $\alpha$ -actin (green in color) and the nuclei with Hoechst (Fig.25). Again, highly aligned myotubes developed on the left side of the construct, whereas fibroblasts developed on the right side. Myotubes also developed on deep levels of the construct, not just on the surface. The approach used allows for a graded tissue suitable for regeneration of the native MTJ.

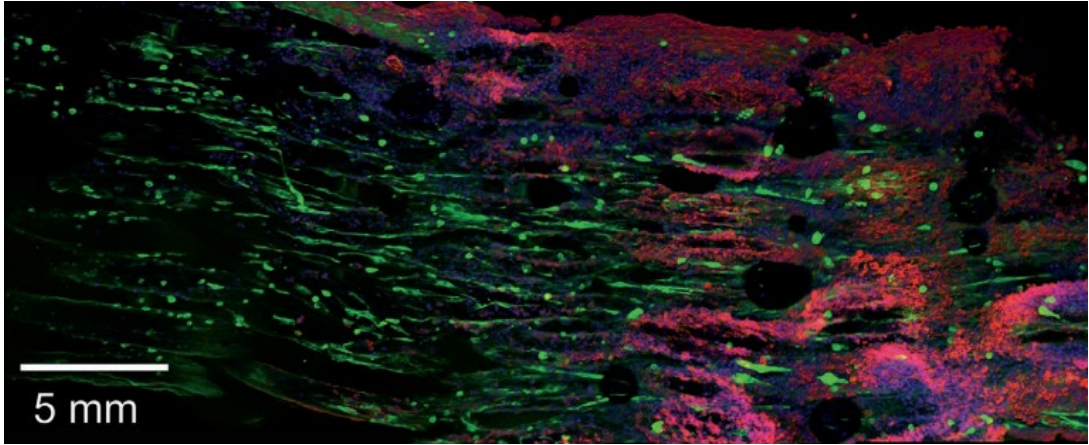


Fig.25 Co-culture of C2C12 myoblasts and NIH/3T3 fibroblasts on flat collagen fiber structures. Confocal image of C2C12 myotubes ( $\alpha$ -actinin, green) and fibroblasts (actin, red) after 7 days of differentiation [88].

## 4.2 3D-PRINTING

In the study by Merceron et Al. (2015) [30] the use of a three-dimensional integrated organ printing (IOP) system is described for the processing and deposition of four different components for the fabrication of a single integrated MTJ construct. Thermoplastic polyurethane (PU) was co-printed with C2C12 cell-laden hydrogel-based bio-ink for elasticity and muscle development on one side, while poly( $\epsilon$ -caprolactone) (PCL) was co-printed with NIH/3T3 cell-laden hydrogel-based bio-ink for stiffness and tendon development on the other. This study demonstrates the versatility of the IOP system to create integrated tissue constructs with region-specific biological and mechanical characteristics for MTJ engineering.

Preparation of cell-laden hydrogel-based bioink and thermoplastic polymers C2C12 myoblasts and NIH/3T3 fibroblasts were used for the fabrication of 3D MTJ constructs.

C2C12 cells were cultured using a high glucose content in Dulbecco's modified eagle medium (DMEM), 20% fetal bovine serum (FBS), and 1% antibiotic or antifungal. NIH/3T3 cells were cultured using high glucose in DMEM culture medium, 10% FBS, and 1% antibiotic or antifungal. Both cells were mixed with a high-viscosity bioink hydrogel consisting of hyaluronic acid, gelatin, and fibrinogen calcium-free high-glucose DMEM. Thermoplastic polyurethane (PU) and poly( $\epsilon$ -caprolactone) (PCL) were used to mimic the mechanical properties of native MTJ tissue.

A 3D computer-aided design (CAD) process was applied to program a 3D IOP system developed in-house, including slicing, tool path generation, and motion program generation. The 3D CAD model was sliced thickly at the microscale to create two-dimensional cross-sections. By combining the information obtained from the two-dimensional section with the conditions of the printing process, including humidity and temperature, a motion program was created that allowed the 3D bioprinter to obtain 3D models by depositing layer-by-layer 2D cross-sectional models containing cells and thermoplastic polymers.

The 3D printer consists of 4 cartridges, two were loaded with thermoplastic structural polymers to act as scaffolds and two were loaded with cell-laden bioinks, to insert the biological component. This system can build customizable fabrics of any shape and tension.

For the "muscle side" PU with C2C12 cells was used, while for the "tendon side" PCL with NIH/3T3 cells was used. The various regions of the MTJ construct are visualized by scanning electron microscopy (SEM) to make an ultrastructural characterization, to do so the substrate was coated with gold sputter (Fig. 26). The mechanical properties of the construct were tested using a tensile testing machine equipped with a 100N load cell. Three specimens were evaluated, one for each region of the construct, the first consisting only of PU, the second consisting only of PCL, and the third consisting of a PU-PCL interface. The thickness and width of each specimen were evaluated using digital calipers and then the specimen was fixed by welding to the clamps of the testing machine. Through this test, stress-strain curves were obtained for each specimen, from which it was possible to calculate the Young Modulus, tensile strength, and strain at the break of each specimen.

Cell viability was assessed using a live dead assay, where live cells were represented by green fluorescence while dead cells were represented by red fluorescence.

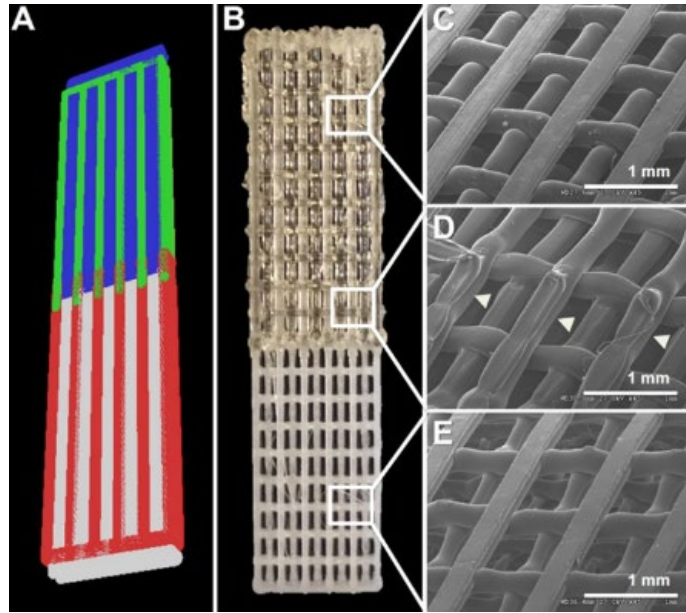


Fig.26. Figure A shows the CAD model of the construct, with the PCL in red, the PU in green, the C2C12 cells in blue, and the NIH/3T3 cells in white. In Figure B we see the actual construct, where the PU side is at the top, the PCL side is at the bottom, and in the middle, there is a 10% overlap interface. In Figure C we see the PU side under the SEM microscope, in Figure D the interface region under the SEM microscope, and Figure E the PCL side under the SEM microscope [30].

The results of the mechanical characterization showed that the PU side had a stress-strain curve typical of elastomeric materials, while the PCL side had a stress-strain curve typical of plastic materials. In addition, the stress-strain curve of PCL had a very short plastic strain (about 10% strain), then it underwent yielding continuing up to 700% strain until it reached failure. The strain-stress curve of the PU-PCL interface presented elastomeric properties up to 300% strain, and then assumed behavior of plastic nature. The PU side presented a Young Modulus of  $0.39 \pm 0.05$  MPa, while the PCL side was much stiffer, with a Young Modulus of  $46.67 \pm 2.67$  MPa. On the other hand, the interface region showed an intermediate value of  $1.03 \pm 0.14$  MPa. The tensile strength did not differ significantly between the samples, while the failure strain showed a significant difference between the PCL and PU sides (Fig.27).

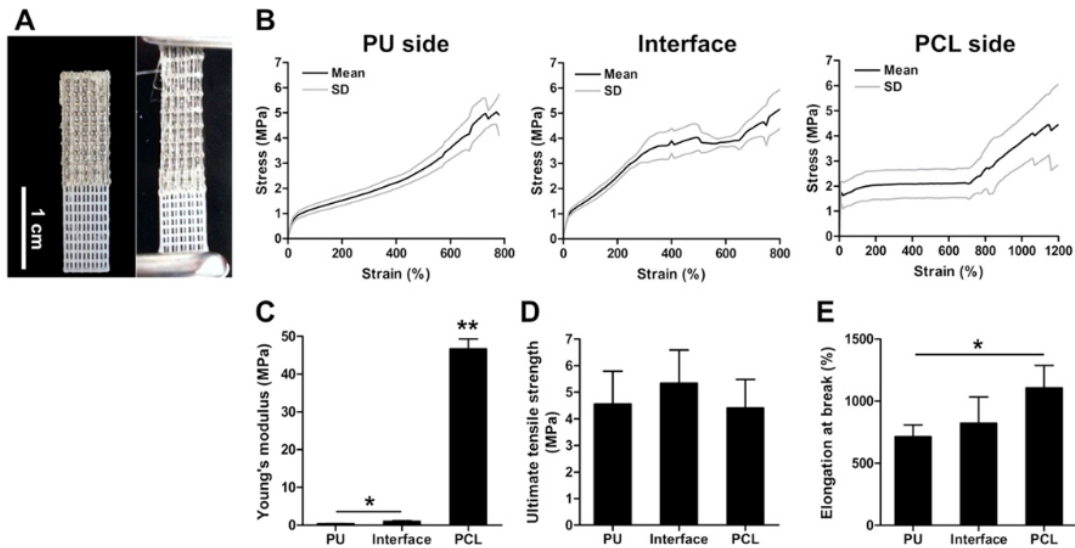


Fig.27 Tensile properties of the bioprinted MTU constructs. (A) When a tensile force is applied, the PU side strains before the PCL side strains. (B) The stress-strain curves of the PU side, interface region, and PCL side. (C) Young Modulus, (D) ultimate tensile strength, and (E) elongation at break of the bioprinted MTU constructs with different regions [30].

Cell viability analysis has shown that after 7 days it is still good and, in addition, C2C12 cells begin to show multinucleation, indicating their differentiation into myotubes; while on the tendon side an initial deposition of collagen I is observed, indicating the production of the main ECM protein that composes the tendon. In addition, cells begin to interact in the interface region, as can be seen in Figure C (yellow color) (Fig.28). It was also verified that the cells began to arrange themselves in an aligned fashion, as typical of native structures.

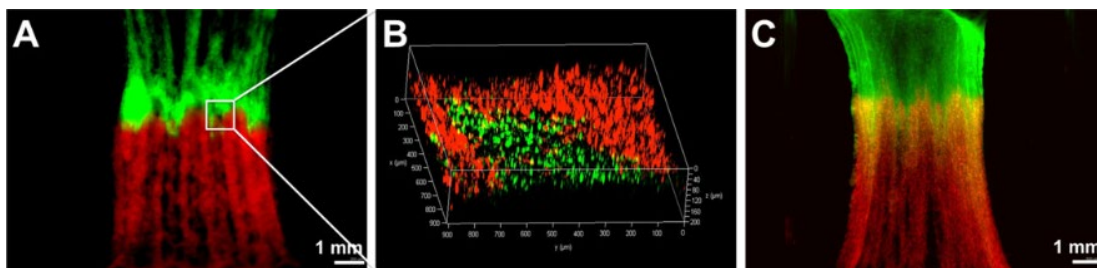


Fig.28 (A)–(C) Fluorescently-labeled dual-cell printed MTU constructs (green: DiO-labeled C2C12 cells; red: DiI-labeled NIH/3T3 cells; yellow: interface region between green and red fluorescence). (A) Constructs were imaged at (A) 1 d and (C) 7 d in culture to show cell-cell interactions and movement. (B) Confocal microscopic image shows a 3D reconstruction of the interface region on 1 d after printing [30].

This study obtained promising results for MTJ regeneration, but it will be necessary to perform mechanical characterizations by placing the construct in a bioreactor, to improve its mechanical properties and verify how the scaffold behaves after several times.

An innovative biofabrication process was used to obtain an MTJ unit in vitro in the study performed by Kim et Al. in 2022 [91]. To obtain the construct, two typical biomaterials, namely, decellularized extracellular matrixes (dECMs) derived from porcine muscle and tendon, and type I collagen were used. To obtain the MTJ unit, it was adapted a 3D bioprinting process supplemented with a newly designed core-sheath nozzle in which a single-core channel and double-sheath channels were composed. The high-weight collagen fraction serves as a mechanical support in the core, while in the sheath, two hASC-containing dECM-based bioinks were used as biological cell-differentiating niche components. In this way, three types of MTJ constructs were obtained so that we could understand which of them best mimicked the native structure. The first type of construct involved direct contact between the muscle and tendon areas. The second type of construct involved a mixed zone of muscle and tendon cells artificially designed while the third type of construct had a zone of contact between muscle and tendon cells in the form of interdigitations (Fig 29).

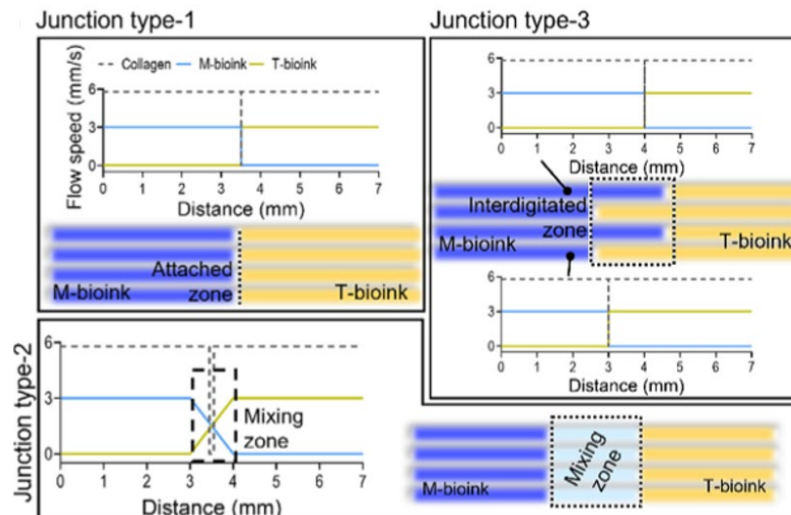


Fig.29 Schematics showing the fabrication procedure for three types of MTJ unit (type 1: direct contact between muscle and tendon, type 2: contact in mixing zone, and type 3: interdigitated contact) [91].

The constructs were subjected to mechanical tensile testing using a testing machine to define their mechanical properties (Fig 30). This testing showed an improvement in mechanical properties with time. Although these properties are lower than expected, it can still be seen that the mechanical properties of the second type of construct are better than those of the other two (Fig 31).

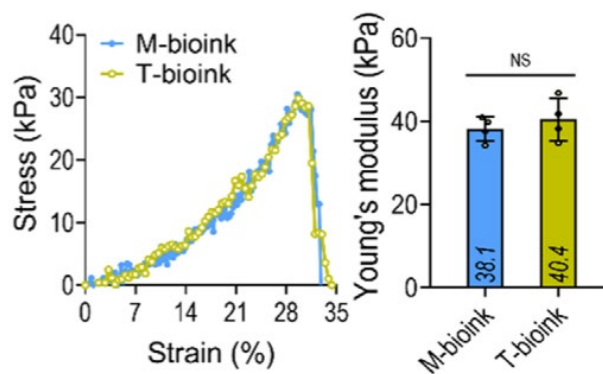


Fig.30 stress-strain curves and Young Modulus for the structures fabricated using M-bioink and T-bioink [91].

The bioprinting process with a single core channel and double sheath channels was used to supply the pure collagen into the core region, and the hASCs containing M-bioink and T-bioink into the sheath regions. By controlling the printing speed and the weight fraction of the collagen, it was possible to control the orientation of the cells, which had to be aligned.

Gene expression evaluation tests showed that the second type of construct shows significantly higher gene expression than the other two constructs. This demonstrates that MTJ development is influenced by the shape of the chosen interface between muscle and tendon cells.

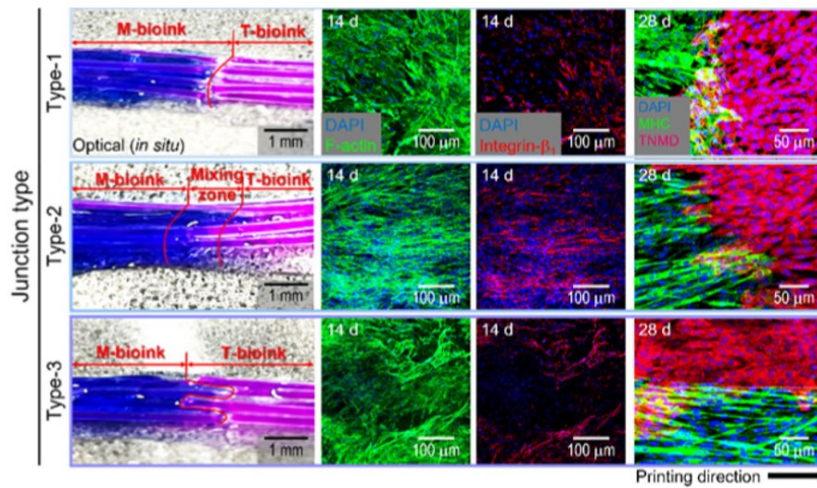


Fig.31 Optical, 406-diamidino-2-phenylindole (DAPI)/F-Actin (at 14 days), DAPI/integrin- $\beta$ 1 (red) (at 14 days), DAPI/F-Actin/integrin- $\beta$ 1 (at 14 days), and DAPI/MHC/TNMD (at 28 days) images for the three types of MTJ interfaces [91].

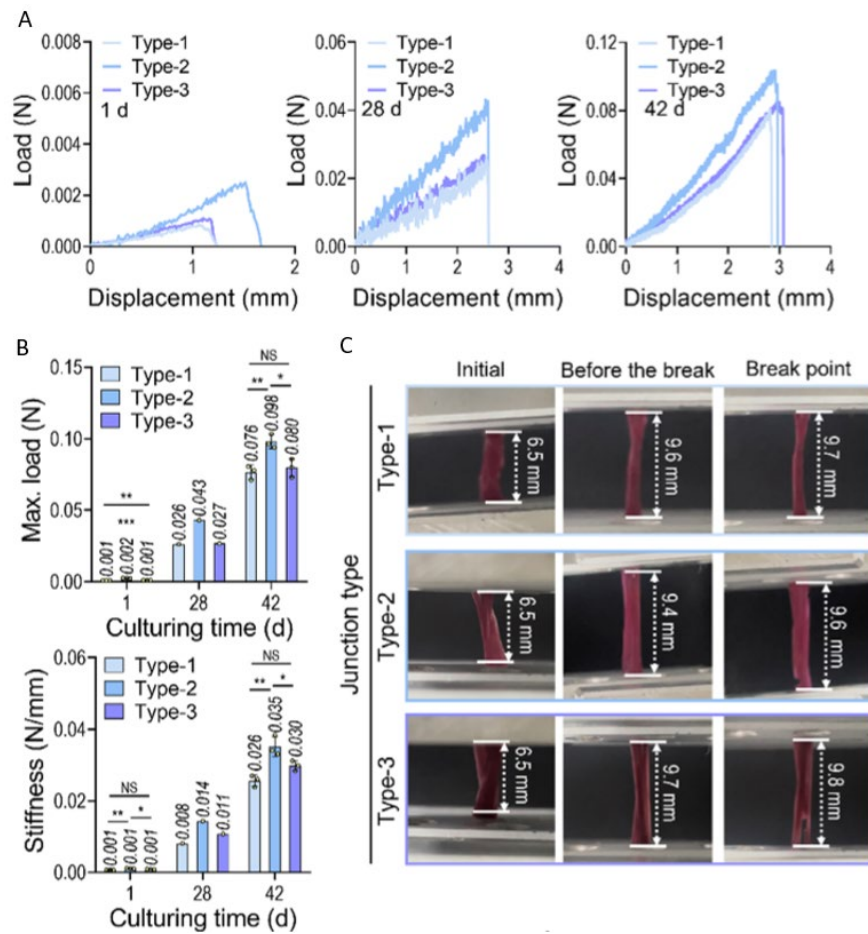


Fig. 32 (A) Load–displacement curves for junction types 1, 2, and 3 at 1, 28, and 42 days of cell culture. (B) The maximum load and stiffness of the myotendinous junction (MTJ) structure were estimated using the load-displacement curves. (C) Captured images of the samples at the initial and breakpoint [91].

A particular technique called assembled cell-decorated collagen (AC-DC) was used to obtain constructs that mimic the native structures of the musculoskeletal system. This innovative technique, used in the study performed by Kyle et Al. [92] in 2022, can obtain constructs with aligned collagen fibers and perform cell seeding on them. Printed implants are formed on rigid temporary supports, which maintain the alignment of the fibers and their 3D macrostructure during the printing process. Fiber dimensions such as length, thickness, and porosity can be controlled using CAD software. A custom extrusion print head is designed and incorporated into a commercial 3D printer. Two separate planetary geared stepper motors with lead screw assemblies mechanically compress disposable syringes individually, extruding cell suspension with sub-microliter resolution.

Multiple cell-solution printheads can prospectively facilitate the production of heterogeneous implants with differing cell populations in distinct regions.

Cell suspensions were prepared in hyaluronic acid solutions and extruded into the seeding manifold during printing. At this point, the cells evenly coat the collagen fiber.

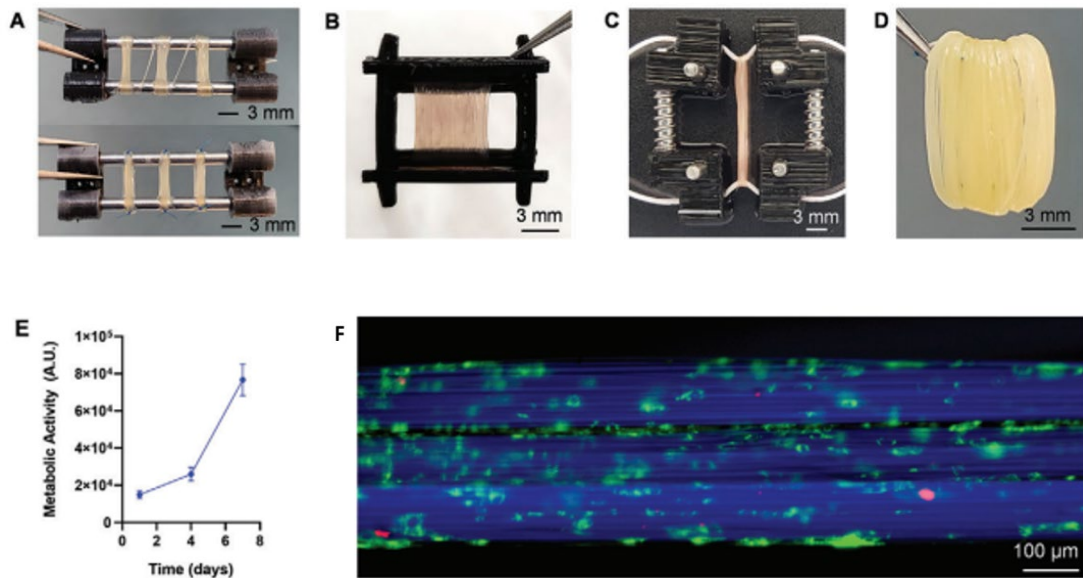


Fig.33 A) Three implants printed on a frame before (top) and after (bottom) being fixed with suture. B) Larger implant printed on a custom frame. C) Implant held in tension by a custom frame, printed on two lengths of suture. D) Implant removed from a frame, secured with suture. E) Fluorescence intensity indicating cell metabolic activity using the alamarBlue assay for implants printed with hMSCs after 1, 4, and 7 d of culture (n = 6). F) Fluorescence image showing hMSCs attached to and distributed along three “building block” strands of collagen fiber after 4 d in culture [92].

To assess cellular metabolic activity, implants were observed using the almarBlue assay after 1, 4, and 7 days of culture. It was observed that cell metabolic activity increased fivefold after 7 days. Furthermore, the cells were distributed in the direction of the collagen fibers.

MSCs were used for cell seeding in biomechanical tests, and the mechanical properties were evaluated after 1 and 28 days of static culture. A custom 2-pin mounting approach for tensile testing was used. The resulting stress-strain curves are shown in Fig.34 with distinct "toe" regions of gradually increasing slope followed by linear regions of maximum slope and ultimately well-defined rapid decreases in stress indicating failure.

The ultimate tensile strength (UTS) and Young Modulus of each construct were evaluated and it was noted that the mechanical properties of the implants were superior to those of the native tendon by several orders of magnitude. Specifically, the values are UTS=20kPa and Young Modulus=200kPa. Moreover, before reaching failure, all implants reached a deformation greater than 20%. Regarding the mechanical properties related to the muscle, it is possible to state that the constructs exceeded those of the native muscle, reaching 0.44MPa of UTS, 2MPa of Young Modulus, and a strain at failure greater than 40%.

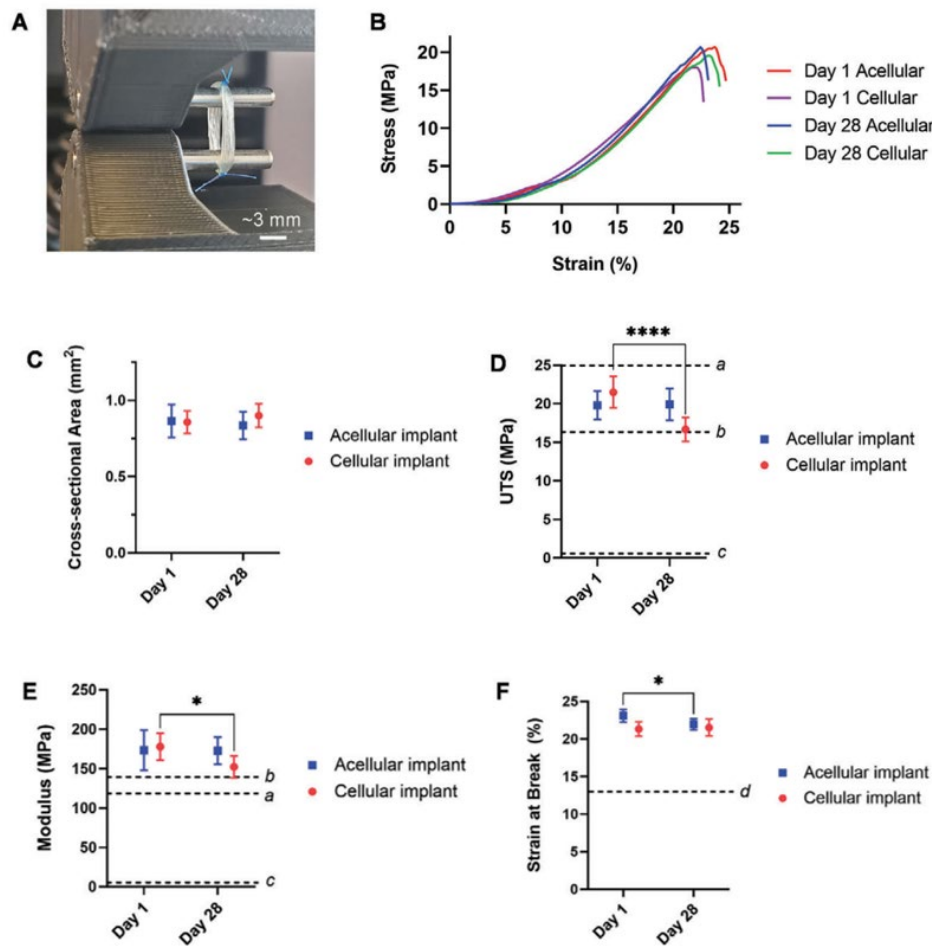


Fig.34 A) A custom two-pin uniaxial tensile testing setup. B) Typical stress-strain curves for each experimental group. C) Measured cross-sectional areas. D) Ultimate tensile stress (UTS). E) Young Modulus. F) Strain at the break. a Mean UTS and Young Modulus of human ACL, b Mean UTS and modulus of the strongest portion of the human supraspinatus tendon, c Mean UTS and modulus of typical collagen gels used in tissue engineering. (All data n = 10 per group per time point \*P < 0.05, \*\*\*\* P < 0.0001 indicates significance) [92].

This bioprinting process is particularly well suited to produce planar, cylindrical, or prismatic geometries. Such geometries are ideal for applications targeting the augmentation or replacement of soft musculoskeletal tissues, where aligned collagen fiber implants mimic the architecture of these native tissues.

This study demonstrated that this bioprinting technique allows for constructs with excellent mechanical properties and directionality that is quite similar to the native one. This suggests that this technique can be used to produce regenerative implants in the field of musculoskeletal injuries, in particular MTJ. Although the studies were performed on an appropriate rodent scale, the processes described can easily be scaled up to produce them on a human scale.

### **4.3 CONSTRUCTS ENGINEERED IN VITRO**

During muscle contraction, for force transmission from the muscle to the tendon to occur properly, the MTJ must remain intact. In a study performed in 2006 by Larkin et Al. [93], the contractile and structural characteristics of 3-D skeletal muscle constructs co-cultured with self-organized tendon constructs or tail tendon segments from adult or fetal mice were evaluated.

Subjecting the MTJ to mechanical characterization increases the expression of several muscles and tendon ECM proteins, including focal adhesion kinase, paxillin, integrin-linked kinase, mitogen-activated protein kinase, and talin [94]. This is very important, as these proteins provide a conduit through which forces are transmitted from muscle to tendon. Failure to express these proteins results in structural damage at the interface during contraction.

To understand whether co-culture led to mechanical interaction between tendon and muscle, the expression of paxillin and talin was used as an indicator. Using Masson's trichrome staining it was possible to follow the morphological development of the co-culture, in blue we see the tendon collagen, the tendon fibroblast nuclei are in a dark color, and in red, there are the multinucleated skeletal muscle cells (Fig.35). It could be seen that after two weeks of co-culture, an interface developed that was quite similar to that of the native MTJ.

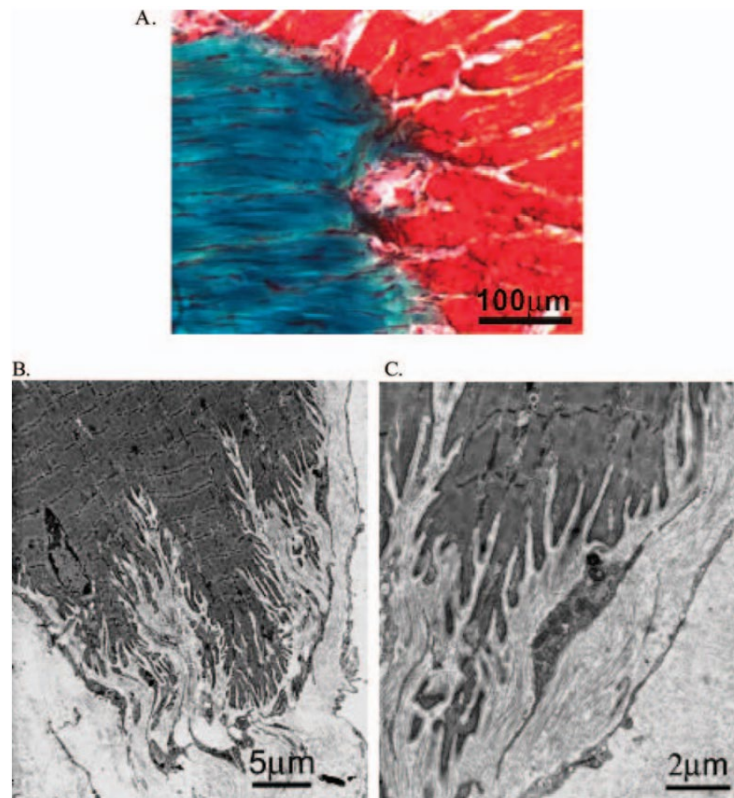


Fig. 35 Frozen sections (A) of normal adult myotendinous junction (MTJ) with Mason's Trichrome staining for tendon collagen (blue), skeletal muscle fibers (red), and cell nuclei (black). Nuclei (dark staining) of fibroblasts in the tendon (tenocytes) are in parallel rows flattened between collagen fibers. Electron micrographs (B and C) of adult MTJs taken at two different magnifications shows the highly digitated interface between muscle and tendon [93].

Subjecting the muscle-tendon construct to mechanical stresses above physiological levels, the interface remains intact, but there is a failure of the structure in the muscle side of the construct. The Young Modulus of the construct is  $37.2\text{kPa} \pm 10.3\text{kPa}$ .

Paxillin expression was detected in the co-culture, this suggests that the constructs were subjected to tensile stress properly. Comparing the expression of paxillin in three different cases (fetal rat MTJ, adult rat MTJ, and engineered MTJ), it was noted that it had a much more prevalent expression in the neonatal MTJ than the adult (Fig.36). Since in the constructs used, paxillin was expressed similarly to neonatal, it means that the constructs are immature. Probably, the engineered construct is not able to reach the adult MTJ phenotype because it is experiencing not enough cyclic loading or because they need more time.

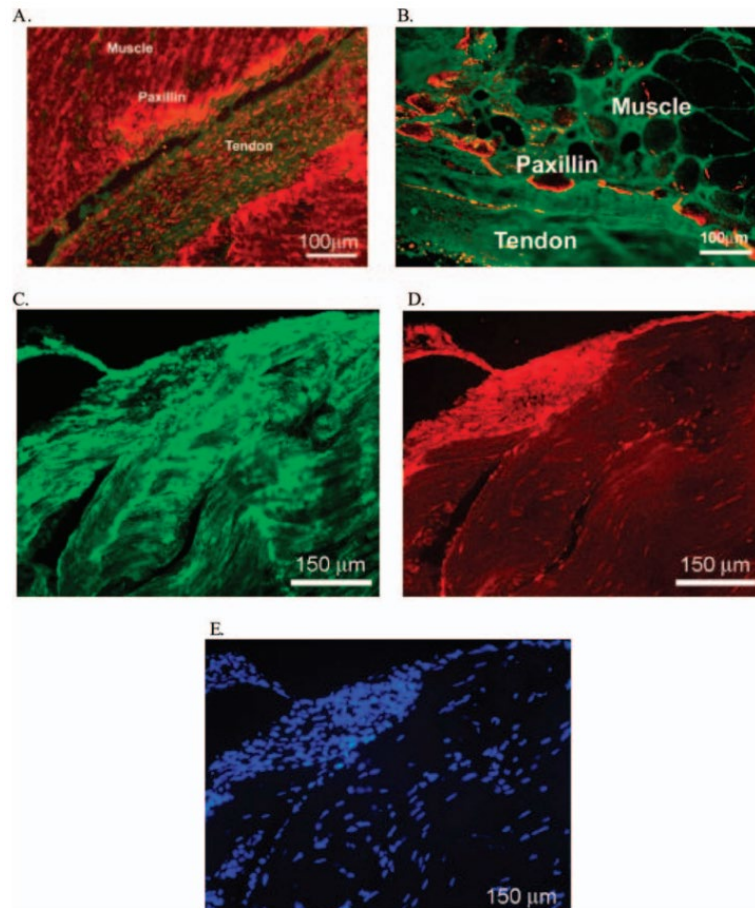


Fig. 36 Immunostaining of adult and fetal myotendinous junctions (MTJs) and the interfaces of the tendon–muscle construct engineered in vitro using adult rat-tail tendon (ART). Paxillin (red) is clustered at the MTJ in (A) neonatal and (B) adult rat muscle. Immunostaining of an ART tendon–muscle construct for (C) type I collagen and (D) paxillin. (E) 40,6-diamidino-2-phenylindole was used to stain nuclei [93].

## **5 DISCUSSIONS**

The MTJ is a very complex anatomical structure, which allows the transmission of the forces generated by the muscle to the tendon structure, to allow movement. Being an interface that connects two very different tissues, on one side the muscle and on the other the tendon, it is very complicated to obtain an artificial structure that can replace it.

These are the main reasons why, even today, the regeneration of the MTJ is still a big challenge for tissue engineering. Among the proposed solutions, the most promising seems to be electrospinning, which can obtain fibers in the nanoscale and can reproduce the hierarchical structure of the tissues that make up the MTJ. Very important is also the choice of materials used, it is necessary to use polymers that can reproduce the mechanical properties of both tissues. But above all, it is important that the two polymers can interact with each other, when put in contact, to form the actual structure of the MTJ.

A crucial factor in the success of a scaffold that can mimic the native structure is the choice of cells. Depending on the cells used, it is possible to develop a structure that mimics the native properties. Since this is an interface structure between two different tissues it is necessary to choose two different types of cell groups, one for muscle and one for tendon. The choices made in the articles described above have been summarized in Table 6.

**Table 6:** Main properties of the analyzed studies (E=Young Modulus; UTS=ultimate tensile strength; SAF=strain at failure).

Study	Cells	Time points	Technique	Mechanical properties	References	Year
Ladd et al.	C2C12 NIH3T3	3,7 days	Electrospinning	UTS: 0.5MPa E: 7.3MPa SAF: 18.5%	[64]	2011
Merceron et al.	C2C12 NIH3T3	1,7 days	3D printing	E: 1.03MPa	[15]	2015
Kishan et al.	hMSCs	3 days	Electrospinning	E: 0.19MPa- 2.39MPa	[71]	2017
Tomas et al.	hASCs	11,21 days	Electrospinning with magneto-mechanical actuation	UTS:4.70 E: 21.55 SAF: 4%	[67]	2019
Koeck et al.	C2C12 NIH3T3	1,3,7 days	Electrospinning	UTS: 241MPa E: 5106MPa SAF: 17%	[66]	2022
Kim et al.	hASCs	14,28 days	3D printing	---	[68]	2022
Kyle et al.	MSCs	1,4,7 days	AC-DC (3D printing)	Tendon side: UTS:20kPa E:200KPa SAF:>20% Muscle side: UTS: 0.44MPa E:2MPa SAF:>40%	[69]	2022

Some of the studies described above seem to be very promising; it has been possible to obtain electrospun structures with materials that are quite similar to the native tissues, especially when electrospun in an aligned fashion. The materials used, in some cases, have been able to interact, forming what appears to resemble the interdigitations typical of MTJ.

Another very promising field is 3D printing, especially MEW, which allows 3D printing with resolution in the nanoscale, using some of the typical principles of electrospinning. This technique merges the fine control of 3D printing on architecture, with the very high resolution of electrospinning, allowing us to obtain very detailed structures. Although no studies using MEW to regenerate MTJ have been described, I believe that this technique could be used in the future to obtain increasingly promising results.

The studies described the importance of subjecting the structures to the mechanical characterization that would increase their mechanical properties emerges. It would therefore be useful to place these structures in bioreactors or subject them to mechanical stimuli, to verify the consequences.

## **6 CONCLUSIONS AND FUTURE PERSPECTIVES**

Through the research carried out, it has been possible to understand that tissue engineering still has much to do in the field of regenerating the interfaces of the musculoskeletal system. Through the studies carried out over the past few years, it is clear that electrospinning is one of the most suitable techniques capable of obtaining hierarchically similar structures to native ones, mainly due to its high resolution.

Special attention needs to be paid to electrospinning techniques that allow structures with graded mechanical properties to be obtained. In the future, to obtain functional structures, the ability of these structures to have spatially graded properties will be crucial. Only in this way will it be possible to replicate the different properties of the tissues that make up interfaces such as the MTJ.

In addition, the native tissues that make up the MTJ exhibit anisotropic mechanical properties. To replicate this important property, it is necessary to use aligned fibers. So, although some of the studies described above have chosen to use random fibers, it is imperative to understand that the use of aligned fibers is a critically important feature.

## 7 REFERENCES

- [1] Visone R, Gilardi M, Marsano A, Rasponi M, Bersini S and Moretti M 2016 Cardiac meets skeletal: What's new in microfluidic models for muscle tissue engineering *Molecules* **21**
- [2] Webb R C 2003 Smooth muscle contraction and relaxation *American Journal of Physiology - Advances in Physiology Education* vol 27 (American Physiological Society) pp 201–6
- [3] Megane Beldjilali-Labro 2020 *Multi-scale analysis and bioinspired approach towards the reconstruction of the myotendinous junction*
- [4] Sensini A, Massafra G, Gotti C, Zucchelli A and Cristofolini L 2021 Tissue Engineering for the Insertions of Tendons and Ligaments: An Overview of Electrospun Biomaterials and Structures *Front Bioeng Biotechnol* **9**
- [5] Gotti C, Sensini A, Zucchelli A, Carloni R and Focarete M L 2020 Hierarchical fibrous structures for muscle-inspired soft-actuators: A review *Appl Mater Today* **20**
- [6] naturali B S *Resistenza dei BioMateriali*
- [7] Janssen I, Heymsfield S B, Wang Z and Ross R 2000 *Skeletal muscle mass and distribution in 468 men and women aged 18-88 yr* vol 89
- [8] Trovato F M, Imbesi R, Conway N and Castrogiovanni P 2016 Morphological and functional aspects of human skeletal muscle *J Funct Morphol Kinesiol* **1** 289–302
- [9] e Lima K M M, Costa Júnior J F S, Pereira W C de A and de Oliveira L F 2018 Assessment of the mechanical properties of the muscle-tendon unit by supersonic shear wave imaging elastography: A review *Ultrasonography* **37** 3–15
- [10] Yoshikawa Y, Yasuike T, Yagi A and Yamada T 1999 Transverse Elasticity of Myofibrils of Rabbit Skeletal Muscle Studied by Atomic Force Microscopy *Biochem Biophys Res Commun* **256** 13–9
- [11] Mathur A B, Truskey G A and Monty Reichert W 2000 Atomic Force and Total Internal Reflection Fluorescence Microscopy for the Study of Force Transmission in Endothelial Cells *Biophys J* **78** 1725–35
- [12] Schleifenbaum S, Schmidt M, Möbius R, Wolfskämpf T, Schröder C, Grunert R, Hammer N and Prietzel T 2016 Load and failure behavior of human muscle samples in the context of proximal femur replacement *BMC Musculoskelet Disord* **17** 149
- [13] Schleifenbaum S, Schmidt M, Möbius R, Wolfskämpf T, Schröder C, Grunert R, Hammer N and Prietzel T 2016 Load and failure behavior of human muscle samples in the context of proximal femur replacement *BMC Musculoskelet Disord* **17** 149
- [14] Hoang P D, Herbert R D, Todd G, Gorman R B and Gandevia S C 2007 Passive mechanical properties of human gastrocnemius muscle–tendon units, muscle fascicles and tendons *in vivo Journal of Experimental Biology* **210** 4159–68
- [15] Toursel T, Stevens L, Granzier H and Mounier Y 2002 Passive tension of rat skeletal soleus muscle fibers: effects of unloading conditions *J Appl Physiol* **92** 1465–72

- [16] Ogneva I v., Lebedev D v. and Shenkman B S 2010 Transversal Stiffness and Young's Modulus of Single Fibers from Rat Soleus Muscle Probed by Atomic Force Microscopy *Biophys J* **98** 418–24
- [17] Defranchi E, Bonaccorso E, Tedesco M, Canato M, Pavan E, Raiteri R and Reggiani C 2005 Imaging and elasticity measurements of the sarcolemma of fully differentiated skeletal muscle fibres *Microsc Res Tech* **67** 27–35
- [18] Bensamoun S, Stevens L, Fleury M J, Bellon G, Goubel F and Ho Ba Tho M C 2006 Macroscopic–microscopic characterization of the passive mechanical properties in rat soleus muscle *J Biomech* **39** 568–78
- [19] Kuthe C D and Uddanwadiker R v. 2016 Investigation of effect of fiber orientation on mechanical behavior of skeletal muscle *J Appl Biomater Funct Mater* **14** 0–0
- [20] Kovanen V, Suominen H and Heikkinen E 1984 Mechanical properties of fast and slow skeletal muscle with special reference to collagen and endurance training *J Biomech* **17** 725–35
- [21] Lv S, Dudek D M, Cao Y, Balamurali M M, Gosline J and Li H 2010 Designed biomaterials to mimic the mechanical properties of muscles *Nature* **465** 69–73
- [22] Lakie M and Robson L G 1988 THIXOTROPY: THE EFFECT OF STRETCH SIZE IN RELAXED FROG MUSCLE *Quarterly Journal of Experimental Physiology* **73** 127–9
- [23] Wolff A v., Niday A K, Voelker K A, Call J A, Evans N P, Granata K P and Grange R W 2006 Passive mechanical properties of maturing extensor digitorum longus are not affected by lack of dystrophin *Muscle Nerve* **34** 304–12
- [24] Moss R L and Halpern W 1977 Elastic and viscous properties of resting frog skeletal muscle *Biophys J* **17** 213–28
- [25] Sensini A and Cristofolini L 2018 Biofabrication of electrospun scaffolds for the regeneration of tendons and ligaments *Materials* **11**
- [26] Murphy W, Black J and Hastings G 2016 *Handbook of biomaterial properties, second edition* (Springer New York)
- [27] Boccaccini A R (Aldo R ) and Gough Julie 2007 *Tissue engineering using ceramics and polymers* (CRC)
- [28] Sharma P and Maffulli N 2005 *Biology of tendon injury: Healing, modeling and remodeling*
- [29] Viidik A 1973 Functional properties of collagenous tissues *Int Rev Connect Tissue Res* **Vol. 6** 127–215
- [30] Merceron T K, Burt M, Seol Y J, Kang H W, Lee S J, Yoo J J and Atala A 2015 A 3D bioprinted complex structure for engineering the muscle-tendon unit *Biofabrication* **7**
- [31] Deng D, Liu W, Xu F, Yang Y, Zhou G, Zhang W J, Cui L and Cao Y 2009 Engineering human neo-tendon tissue in vitro with human dermal fibroblasts under static mechanical strain *Biomaterials* **30** 6724–30

- [32] Valentin J E, Turner N J, Gilbert T W and Badylak S F 2010 Functional skeletal muscle formation with a biologic scaffold *Biomaterials* **31** 7475–84
- [33] Levenberg S, Rouwkema J, Macdonald M, Garfein E S, Kohane D S, Darland D C, Marini R, van Blitterswijk C A, Mulligan R C, D'Amore P A and Langer R 2005 Engineering vascularized skeletal muscle tissue *Nat Biotechnol* **23** 879–84
- [34] Kuo I Y and Ehrlich B E 2015 Signaling in muscle contraction *Cold Spring Harb Perspect Biol* **7**
- [35] Tidball J G and Chan M 1989 *Adhesive strength of single muscle cells to basement membrane at myotendinous junctions*
- [36] Charvet B, Ruggiero F and le Guellec D 2012 *The development of the myotendinous junction. A review vol 2*
- [37] Zhao C, Wang S, Wang G, Su M, Song L, Chen J, Fan S and Lin X 2018 Preparation of decellularized biphasic hierarchical myotendinous junction extracellular matrix for muscle regeneration *Acta Biomater* **68** 15–28
- [38] Bechtold J E, Eastlund D T, Butts M K, Lagerborg D F and Kyle R F 1994 The Effects of Freeze-drying and Ethylene Oxide Sterilization on the Mechanical Properties of Human Patellar Tendon *Am J Sports Med* **22** 562–6
- [39] Johnson G A, Tramaglino D M, Levine R E, Ohno K, Choi N-Y and L-Y. Woo S 1994 Tensile and viscoelastic properties of human patellar tendon *Journal of Orthopaedic Research* **12** 796–803
- [40] Lännergren J 1971 The Effect of Low-Level Activation on the Mechanical Properties of Isolated Frog Muscle Fibers *Journal of General Physiology* **58** 145–62
- [41] Halpern W and Moss R 1976 Elastic modulus and stress relationships in stretched and shortened frog sartorii *American Journal of Physiology-Legacy Content* **230** 205–10
- [42] Moss R L and Halpern W 1977 Elastic and viscous properties of resting frog skeletal muscle *Biophys J* **17** 213–28
- [43] Kovanen V, Suominen H and Heikkinen E 1984 Mechanical properties of fast and slow skeletal muscle with special reference to collagen and endurance training *J Biomech* **17** 725–35
- [44] Lakie M and Robson L G 1988 THIXOTROPY: THE EFFECT OF STRETCH SIZE IN RELAXED FROG MUSCLE *Quarterly Journal of Experimental Physiology* **73** 127–9
- [45] Lieber R L, Leonard M E, Brown C G and Trestik C L 1991 Frog semitendinosus tendon load-strain and stress-strain properties during passive loading *American Journal of Physiology-Cell Physiology* **261** C86–92
- [46] Wolff A v., Niday A K, Voelker K A, Call J A, Evans N P, Granata K P and Grange R W 2006 Passive mechanical properties of maturing extensor digitorum longus are not affected by lack of dystrophin *Muscle Nerve* **34** 304–12
- [47] Ladd M R, Lee S J, Stitzel J D, Atala A and Yoo J J 2011 Co-electrospun dual scaffolding system with potential for muscle-tendon junction tissue engineering *Biomaterials* **32** 1549–59

- [48] Vila Pouca M C P, Parente M P L, Jorge R M N and Ashton-Miller J A 2021 Injuries in Muscle-Tendon-Bone Units: A Systematic Review Considering the Role of Passive Tissue Fatigue *Orthop J Sports Med* **9**
- [49] Meimandi-Parizi A, Oryan A and Moshiri A 2013 Role of tissue engineered collagen based tridimensional implant on the healing response of the experimentally induced large Achilles tendon defect model in rabbits: A long term study with high clinical relevance *J Biomed Sci* **20**
- [50] Moshiri A and Oryan A 2012 Role of tissue engineering in tendon reconstructive surgery and regenerative medicine: Current concepts, approaches and concerns *Hard Tissue* **1**
- [51] Oryan A, Moshiri A and Meimandi-Parizi A *Graft selection in ACL reconstructive surgery: past, present, and future*
- [52] Park Y S and Sung K S 2012 Surgical reconstruction of chronic achilles tendon ruptures using various methods *Orthopedics* **35**
- [53] Maffulli N, Spiezia F, Testa V, Capasso G, Longo U G and Denaro V 2012 Free gracilis tendon graft for reconstruction of chronic tears of the Achilles tendon *Journal of Bone and Joint Surgery - Series A* **94** 906–10
- [54] Ronel D N, Newman M I, Gayle L B and Hoffman L A 2004 Recent advances in the reconstruction of complex Achilles tendon defects *Microsurgery* **24** 18–23
- [55] Beals T C, Severson E P, Kinikini D and Aoki S *Complex Achilles Reconstruction for Massive Soft Tissue Loss: Allograft, Autograft, and Use of a Temporary Cement Spacer*
- [56] Moshiri A, Oryan A and Meimandi-Parizi A 2013 Role of tissue-engineered artificial tendon in healing of a large achilles tendon defect model in rabbits *J Am Coll Surg* **217**
- [57] Palmer E M, Beilfuss B A, Nagai T, Semnani R T, Badylak S F and van Seventer G A 2002 *Human Helper T Cell Activation and Differentiation Is Suppressed by Porcine Small Intestinal Submucosa* vol 8
- [58] Pridgen B C, Woon C Y L, Kim M, Thorfinn J, Lindsey D, Pham H and Chang J 2011 Flexor tendon tissue engineering: Acellularization of human flexor tendons with preservation of biomechanical properties and biocompatibility *Tissue Eng Part C Methods* **17** 819–28
- [59] Veillette C J ; C K D ; H D A ; F M J ; F C B 1998 Localization and characterization of porcine patellar tendon xenograft antigens in a rabbit model of medial collateral ligament replacement *Transplantation* **65** 486–93
- [60] Moshiri A 2013 Tendon and Ligament Tissue Engineering, Healing and Regenerative Medicine *J Sports Med Doping Stud* **03**
- [61] Cornwell K G, Landsman A and James K S 2009 Extracellular Matrix Biomaterials for Soft Tissue Repair *Clin Podiatr Med Surg* **26** 507–23
- [62] Bonnevie E D and Mauck R L 2018 Physiology and Engineering of the Graded Interfaces of Musculoskeletal Junctions

- [63] Langer R 2000 Biomaterials in drug delivery and tissue engineering: One laboratory's experience *Acc Chem Res* **33** 94–101
- [64] O'Brien 2011 *Biomaterials & scaffolds for tissue engineering*
- [65] Hollister S J 2005 *Porous scaffold design for tissue engineering*
- [66] Causa F, Netti P A and Ambrosio L 2007 A multi-functional scaffold for tissue regeneration: The need to engineer a tissue analogue *Biomaterials* **28** 5093–9
- [67] Sung H J, Meredith C, Johnson C and Galis Z S 2004 The effect of scaffold degradation rate on three-dimensional cell growth and angiogenesis *Biomaterials* **25** 5735–42
- [68] Chevalier E, Chulia D, Pouget C and Viana M 2008 Fabrication of porous substrates: A review of processes using pore forming agents in the biomaterial field *J Pharm Sci* **97** 1135–54
- [69] Loh Q L and Choong C 2013 Three-dimensional scaffolds for tissue engineering applications: Role of porosity and pore size *Tissue Eng Part B Rev* **19** 485–502
- [70] Teo W E and Ramakrishna S 2006 A review on electrospinning design and nanofibre assemblies *Nanotechnology* **17**
- [71] Huang Z M, Zhang Y Z, Kotaki M and Ramakrishna S 2003 A review on polymer nanofibers by electrospinning and their applications in nanocomposites *Compos Sci Technol* **63** 2223–53
- [72] Xue J, Xie J, Liu W and Xia Y 2017 Electrospun Nanofibers: New Concepts, Materials, and Applications *Acc Chem Res* **50** 1976–87
- [73] Haider A, Haider S and Kang I K 2018 A comprehensive review summarizing the effect of electrospinning parameters and potential applications of nanofibers in biomedical and biotechnology *Arabian Journal of Chemistry* **11** 1165–88
- [74] Anon *Electrostatic Spinning of Acrylic Microfibers*
- [75] Matabola K P and Moutloali R M 2013 The influence of electrospinning parameters on the morphology and diameter of poly(vinylidene fluoride) nanofibers- Effect of sodium chloride *J Mater Sci* **48** 5475–82
- [76] Wang T and Kumar S 2006 Electrospinning of polyacrylonitrile nanofibers *J Appl Polym Sci* **102** 1023–9
- [77] Sill T J and von Recum H A 2008 Electrospinning: Applications in drug delivery and tissue engineering *Biomaterials* **29** 1989–2006
- [78] Jarusuwannapoom T, Hongrojjanawiwat W, Jitjaicham S, Wannatong L, Nithitanakul M, Pattamaprom C, Koombhongse P, Rangkupan R and Supaphol P 2005 Effect of solvents on electro-spinnability of polystyrene solutions and morphological appearance of resulting electrospun polystyrene fibers *Eur Polym J* **41** 409–21
- [79] Reneker D H and Yarin A L 2008 Electrospinning jets and polymer nanofibers *Polymer (Guildf)* **49** 2387–425
- [80] O'Connor R A and McGuinness G B 2016 Electrospun nanofibre bundles and yarns for tissue engineering applications: A review *Proc Inst Mech Eng H* **230** 987–98

- [81] Brennan D A, Conte A A, Kanski G, Turkula S, Hu X, Kleiner M T and Beachley V 2018 Mechanical Considerations for Electrospun Nanofibers in Tendon and Ligament Repair *Adv Healthc Mater* **7**
- [82] Wei L and Qin X 2016 Nanofiber bundles and nanofiber yarn device and their mechanical properties: A review *Textile Research Journal* **86** 1885–98
- [83] Shirazi S F S, Gharekhani S, Mehrali M, Yarmand H, Metselaar H S C, Adib Kadri N and Osman N A A 2015 A review on powder-based additive manufacturing for tissue engineering: Selective laser sintering and inkjet 3D printing *Sci Technol Adv Mater* **16**
- [84] Boland T, Xu T, Damon B and Cui X 2006 Application of inkjet printing to tissue engineering *Biotechnol J* **1** 910–7
- [85] Fina F, Goyanes A, Gaisford S and Basit A W 2017 Selective laser sintering (SLS) 3D printing of medicines *Int J Pharm* **529** 285–93
- [86] Gungor-Ozkerim P S, Inci I, Zhang Y S, Khademhosseini A and Dokmeci M R 2018 Bioinks for 3D bioprinting: An overview *Biomater Sci* **6** 915–46
- [87] Hugenberg N R, Dong L, Cooper J A, Corr D T and Oberai A A 2020 Characterization of spatially graded biomechanical scaffolds *J Biomech Eng* **142**
- [88] Koeck K S, Salehi S, Humenik M and Scheibel T 2021 Processing of Continuous Non-Crosslinked Collagen Fibers for Microtissue Formation at the Muscle-Tendon Interface *Adv Funct Mater*
- [89] Kishan A P, Robbins A B, Mohiuddin S F, Jiang M, Moreno M R and Cosgriff-Hernandez E M 2017 Fabrication of macromolecular gradients in aligned fiber scaffolds using a combination of in-line blending and air-gap electrospinning *Acta Biomater* **56** 118–28
- [90] Tomás A R, Gonçalves A I, Paz E, Freitas P, Domingues R M A and Gomes M E 2019 Magneto-mechanical actuation of magnetic responsive fibrous scaffolds boosts tenogenesis of human adipose stem cells *Nanoscale* **11** 18255–71
- [91] Kim W J and Kim G H 2022 A bioprinted complex tissue model for myotendinous junction with biochemical and biophysical cues *Bioeng Transl Med*
- [92] Christensen K W, Turner J, Coughenour K, Maghdouri-White Y, Bulysheva A A, Sergeant O, Rariden M, Randazzo A, Sheean A J, Christ G J and Francis M P 2022 Assembled Cell-Decorated Collagen (AC-DC) Fiber Bioprinted Implants with Musculoskeletal Tissue Properties Promote Functional Recovery in Volumetric Muscle Loss *Adv Healthc Mater* **11**
- [93] Larkin L M, Calve S, Kostrominova T Y and Arruda E M *Structure and Functional Evaluation of Tendon-Skeletal Muscle Constructs Engineered in Vitro*
- [94] Gordon S E, Flu"ck M, Flu"ck F, Booth F W, Fl"u M and Booth F W 2001 *Selected Contribution: Skeletal muscle focal adhesion kinase, paxillin, and serum response factor are loading dependent* vol 90

## **RINGRAZIAMENTI**

Ringrazio primo fra tutti il Prof. Sensini, per il suo fondamentale supporto, per la grande disponibilità e per la professionalità che ha sempre dimostrato. I suoi insegnamenti sono stati una grande ispirazione.

A mamma e papà, al loro costante sostegno, ai loro insegnamenti e ai loro consigli, senza i quali oggi non sarei ciò che sono. Senza di voi tutto questo non sarebbe stato possibile.

Alle mie sorelle, Asia e Arianna, per avermi sempre portato gioia ed allegria. Spero di essere un buon esempio a cui ispirarsi.

A Petar, compagno di vita. Grazie per amarmi per ciò che sono e per essere sempre al mio fianco, soprattutto nei momenti difficili. Grazie per avermi supportata e sopportata giorno dopo giorno.

A Camilla, la mia compagna di avventure. Grazie per aver gioito con me dei traguardi raggiunti.

Un grazie speciale anche a tutti i miei amici, che hanno incrociato la loro vita con la mia lasciandomi qualcosa di buono.

Infine, ringrazio me stessa, ai miei sacrifici e alla mia tenacia che mi hanno fatta arrivare fin qui.